

Supporting Information

Increasing phosphorescent quantum yields and lifetimes of platinum-alkynyl complexes with extended conjugation

Yuzhen Zhang, Cory E. Hauke, Matthew R. Crawley, Bradley E. Schurr, Cressa Ria P. Fulong,
Timothy R. Cook*

Department of Chemistry, University at Buffalo, State University of New York, Buffalo, New York 14260, United States

Table of Contents

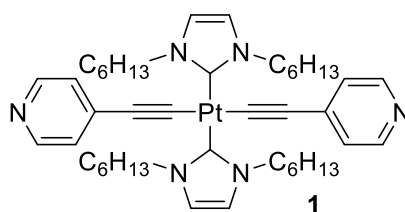
Experimental Information	Page S2
^1H, $^{13}\text{C}\{^1\text{H}\}$, and $^{31}\text{P}\{^1\text{H}\}$ NMR	Page S7
Photophysical Details	Page S16
Luminescence Decay Traces	Page S16
Emission and Excitation Spectra	Page S20
Computation Details	Page S22
Computational Results	Page S22
Crystallographic Details	Page S44
References	Page S46

Experimental Details

General Information

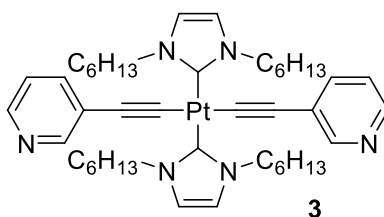
All reactions were carried out by using standard Schlenk techniques under nitrogen inert atmosphere. All reagents were used as received unless otherwise stated. Solvent was purified by Pure Process Technology (Nashua, NH) freestanding solvent purification system. ^1H and $^{13}\text{C}\{^1\text{H}\}$ spectra were recorded on Varian 300, 400 or 500 MHz spectrometers. Chemical shifts (δ) are reported in parts per million (ppm) referenced to tetramethylsilane (δ 0.00) ppm using the residual protio solvent peaks as internal standards (^1H NMR experiments) or the characteristic resonances of the solvent nuclei (^{13}C NMR experiments). Coupling constants (J) are quoted in Hertz (Hz), and the following abbreviations are used to describe the signal multiplicities: s (singlet); d (doublet); t (triplet); q (quartet); m (multiplet). Infrared (IR) spectra were recorded on a Perkin Elmer 1760 FTIR spectrometer with frequencies (ν_{max}) quoted in wavenumbers (cm^{-1}). Mass spectra were run on LCQ Advantage IonTrap LC/MS. TLC analyses were performed on pre-coated Merck Silica Gel60F254 slides and visualized by luminescence quenching either at (short wavelength) 254 nm or (long wavelength) 365 nm. Chromatographic purification of products was performed on a short column (length 15.0 cm, diameter 1.5 cm) using silica gel 60, 230–400 mesh using a forced flow of eluent.

trans-[Pt(dhim) $_2$ I $_2$],¹ *trans*-Pt(PEt $_3$) $_2$ I $_2$,² and Pt(PEt $_3$) $_2$ (C \equiv C-4-Py) $_2$ ³ (**2**) were synthesized by following reported protocols. 3-ethynyl pyridine, 4-ethynyl pyridine hydrochloride and 1,3-di(cyclohexyl) imidazolium chloride are commercial available from AK Scientific Inc.



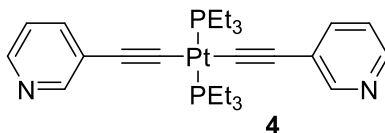
trans-[Pt(dhim) $_2$ (C \equiv C-4-Py) $_2$] **1**. Precursor *trans*-[Pt(dhim) $_2$ I $_2$] (739 mg, 1.00 mmol), 4-ethynylpyridine hydrochloride (321 mg, 2.30 mmol) were placed in a 250 mL Schleck flask. Diethylamine (20.0 mL) and dichloromethane (40.0 mL) were added to dissolve the reactants. The

solution was purged with nitrogen for 10 minutes and CuI (20 mg, 0.10 mmol) was added. The mixture was stirred under dark overnight. H₂O was added to quench the reaction. CH₂Cl₂ was used to extract and the organic phase was collected, dried by MgSO₄ and purified by silica gel column chromatography with eluent of CH₂Cl₂: MeOH (49:1). 702 mg (80%) colorless product was obtained. ¹H NMR (400 MHz, CD₂Cl₂, 25 °C): δ (ppm) = 8.28 (d, 4H, ³J = 6.0 Hz, pyridinyl), 7.00 (s, 4H, imidazole), 6.96 (d, 4H, ³J = 6.0 Hz, pyridinyl), 4.46 (t, 8H, ³J = 8.0 Hz, NCH₂CH₂), 2.08 (t, 8H, ³J = 8.0 Hz, NCH₂CH₂), 1.45 (m, 8H, NCH₂CH₂CH₂), 1.34 (m, 16H, CH₂CH₂CH₃), 0.91 (m, 12H, ³J = 8.0 Hz, CH₃); ¹³C{¹H} NMR (75.4 MHz, CD₂Cl₂, 25 °C): δ (ppm) = 168.49 (C=Pt), 148.70, 136.79, 125.41, 119.95 (NCHCHN), 117.11 (Pyridinyl), 104.29 (C≡C), 50.91, 31.64, 30.67, 26.61, 22.63 (C on (CH₂)₅CH₃), 13.76 (CH₃); ESI-MS *m/z*: 873.5 [M + 2H]⁺, 436.7 [M + 2H]²⁺ (M = C₄₄H₆₄N₆Pt). IR (ATR, cm⁻¹) $\tilde{\nu}_{C\equiv C}$ = 2090. E. A. Pred.: C 60.6% H 7.61% N 9.61% Found: C 61.1%, H 7.4%, N 9.8%



***trans*-[Pt(dhim)₂(C≡C-3-Py)₂] 3.** *trans*-[Pt(dhim)₂I₂] (400 mg, 0.434 mmol), 3-ethynylpyridine (181.8 mg, 1.303 mmol) were placed in a 250 mL Schleck flask. Diisopropylamine (10.0 mL) and THF (40.0 mL) were added to dissolve the reactants. The solution was purged with nitrogen for 10 minutes and CuI (10 mg, 0.05 mmol) was added. The mixture was stirred at reflux condition under dark for 24 hrs. H₂O was added to quench the reaction. CH₂Cl₂ was used to extract and the organic phase was collected, dried by MgSO₄ and purified by silica gel column chromatography with eluent of CH₂Cl₂: MeOH (97:3), then purified again by alumina column with eluent of CH₂Cl₂:MeOH (99:1). The solid was recrystallized with ether and CH₂Cl₂. 167 mg (44%) colorless product was obtained. ¹H NMR (400 MHz, CDCl₃, 25 °C): δ (ppm) = 8.30 (s, 2H, pyridinyl), 8.20 (d, 2H, ³J = 6.0 Hz, pyridinyl), 7.33 (d, 2H, ³J = 6.0 Hz, pyridinyl), 6.97 (t, 2H, ³J = 6.0 Hz, pyridinyl), 6.87 (s, 4H, imidazole), 4.43 (t, 8H, ³J = 8.0 Hz, NCH₂CH₂), 2.03 (m, 8H, ³J = 8.0 Hz, NCH₂CH₂), 1.38 (m, 8H, NCH₂CH₂CH₂), 1.25 (m, 16H, CH₂CH₂CH₃), 0.81 (m, 12H, ³J = 8.0 Hz, CH₃); ¹³C{¹H} NMR (75.4 MHz, CDCl₃, 25 °C): δ (ppm) = 169.08 (C-Pt), 152.35, 144.45, 137.42, 122.33, 119.67 (NCHCHN), 112.50 (C≡C), 102.13 (C≡C), 50.97,

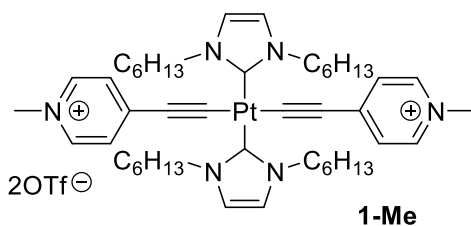
31.62, 30.65, 26.66, 22.62 (C on $(\text{CH}_2)_5\text{CH}_3$), 13.99 (CH_3); ESI-MS m/z : 872.5 $[\text{M} + \text{H}]^+$, 437.5 $[\text{M} + 2\text{H}]^{2+}$ ($\text{M} = \text{C}_{44}\text{H}_{64}\text{N}_6\text{Pt}$). IR (ATR, cm^{-1}) $\tilde{\nu}_{\text{C}=\text{C}} = 2087$. E. A. Pred.: C 60.6% H 7.6% N 9.6% Found: C 61.1%, H 7.4%, N 9.6%



trans-[Pt(PEt₃)₂(C≡C-3-Py)₂] 4. *trans*-Pt(PEt₃)₂I₂ (300 mg, 0.430 mmol), 3-ethynylpyridine (100 mg, 0.960 mmol) and CuI (8.00 mg, 0.043 mmol) were placed into a 200 ml Schlenk flask under nitrogen. Then 25.0 mL CH₂Cl₂ and 5.0 mL trimethylamine were added under nitrogen. The mixture was stirring in the dark overnight at room temperature and a white precipitate of triethylammonium iodide appeared. After removing precipitate by filtration, the solvent was removed on a rotary evaporator, and the product was purified by column chromatography on silica gel with eluent of CH₂Cl₂/MeOH (99:1). The product was recovered as light yellow compound (200 mg, 72%). ¹H NMR (CDCl₃, 300 MHz, 25 °C): δ (ppm) = 8.51 (s, 2H, pyridinyl), 8.33 (d, 2H, pyridinyl), 7.52 (d, 2H, ³J = 8.0 Hz, pyridinyl), 7.12 (t, 2H, pyridinyl), 2.21 (m, 12H, PCH₂CH₃), 1.27 (m, 12H, PCH₂CH₃); ³¹P{¹H} NMR (CDCl₃, 121.5 MHz, 25 °C): δ (ppm) = 11.02 (*J*_{Pt-P} = 2351 Hz). ¹³C{¹H} NMR (75.5 MHz, CDCl₃, 25 °C): δ (ppm) = 151.93, 145.46, 137.28, 125.41, 122.75, 112.00, 106.06, 16.35, 8.32; ESI-MS m/z : 636.2 $[\text{M} + \text{H}]^{1+}$, ($\text{M} = \text{C}_{26}\text{H}_{38}\text{N}_2\text{P}_2\text{Pt}$). IR (ATR, cm^{-1}) $\tilde{\nu}_{\text{C}=\text{C}} = 2102$. E. A. Pred.: C 49.1% H 6.0% N 4.4% Found: C 48.7%, H 6.1%, N 4.6%

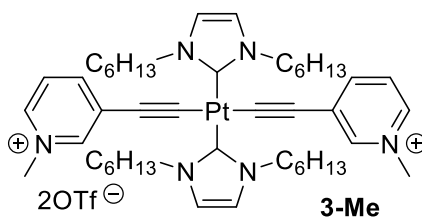
General procedure for methylation.

The procedure for methylation is the same for each molecule and details are given for methylation of **1** to form **2**, only.

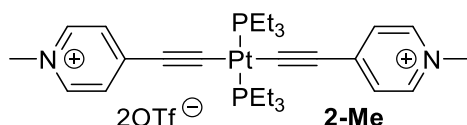


trans-[Pt(dhim)₂(C≡C-4-C₅H₄NCH₃)₂]·2SO₃CF₃ 1-Me. *trans*-[Pt(dhim)₂(C≡C-4-py)₂] **1** (27.44 mg, 0.0300 mmol) were placed in a 50 mL Schleck flask and dissolved with 5 mL dry CH₂Cl₂

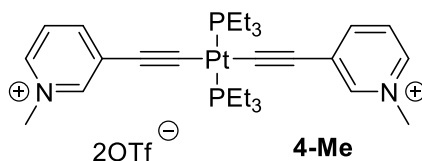
under N₂. Then the flask was sealed and cooled down to 0 °C with ice bath. Methyl trifluoromethanesulfonate (129 mg, 85.0 μL) was added by a syringe. The mixture was stirred under N₂ by covering of aluminum foil for 2 hours at 0 °C. The solution was concentrated to 2 mL and hexanes/ ether was added to precipitate out light yellow solid. The solid was collected and washed with ether two times. The product was dried under high vacuum and 23 mg (68%) yellow product was obtained. ¹H NMR (500 MHz, CD₂Cl₂, 25 °C): δ (ppm) = 8.36 (d, 4H, ³J = 7.0 Hz, pyridinyl), 7.35 (d, 4H, ³J = 7.0 Hz, pyridinyl), 7.05 (s, 4H, imidazole), 4.39 (t, 8H, ³J = 8.0 Hz, NCH₂CH₂), 4.31 (s, 6H, NCH₃), 2.00 (t, 8H, ³J = 7.0 Hz, NCH₂CH₂), 1.40 (m, 8H, NCH₂CH₂CH₂), 1.30 (m, 16H, CH₂CH₂CH₃), 0.85 (m, 12H, ³J = 7.0 Hz, CH₃); ¹³C{¹H} NMR (128.8 MHz, CD₂Cl₂, 25 °C): δ (ppm) = 165.12 (C-Pt), 145.37, 143.10, 128.90 (Pyridinyl), 120.67 (NCHCHN), 108.14 (C≡C), 47.32(NCH₃), 31.56, 30.70, 26.44, 22.59 (C on (CH₂)₅CH₃), 13.78 (CH₃); ESI-MS *m/z*: 1051.4 [M – OTf]⁺, 450.7 [M – 2OTf]²⁺, (M = C₄₈H₇₀F₆N₆O₆PtS₂). IR (ATR, cm⁻¹) $\tilde{\nu}_{C\equiv C}$ = 2065. E. A. Pred.: C 48.0% H 5.9% N 7.0% Found: C 47.5%, H 5.6%, N 6.9%



***trans*-[Pt(dhim)₂(C≡C-3-C₅H₄NCH₃)₂]·2SO₃CF₃ 3-Me.** The temperature was maintained at –10 °C and colorless product was obtained with yield of 78%. ¹H NMR (400 MHz, CD₂Cl₂, 25 °C): δ (ppm) = 8.53 (d, 2H, ³J = 8.0 Hz, pyridinyl), 8.09 (s, 2H, pyridinyl), 7.90 (d, 2H, ³J = 8.0 Hz, pyridinyl), 7.70, (t, 2H, pyridinyl), 7.02 (s, 4H, imidazole), 4.37 (t, 8H, ³J = 8.0 Hz, NCH₂CH₂), 4.22 (s, 6H, NCH₃), 2.05 (t, 8H, ³J = 7.0 Hz, NCH₂CH₂), 1.43 (m, 8H, NCH₂CH₂CH₂), 1.34 (m, 16H, CH₂CH₂CH₃), 0.90 (m, 12H, ³J = 7.0 Hz, CH₃); ¹³C{¹H} NMR (75.5 MHz, CD₂Cl₂, 25 °C): δ (ppm) = 166.51 (C=Pt), 145.75, 145.10, 139.85, 130.48, 127.36, 126.28, 122.96, 120.46, 118.71, 99.48, 50.89, 48.54, 31.64, 30.73, 26.48, 22.63, 13.79; ESI-MS *m/z*: 1051.4 [M – OTf]⁺, 450.7 [M – 2OTf]²⁺, (M = C₄₈H₇₀F₆N₆O₆PtS₂). IR (ATR, cm⁻¹) $\tilde{\nu}_{C\equiv C}$ = 2065. E. A. Pred.: C 48.0% H 5.9% N 7.0% Found: C 48.0%, H 5.7%, N 7.0%



***trans*-[Pt(PEt₃)₂(C≡C-4-C₅H₄NCH₃)₂]**·2SO₃CF₃ 2-Me.** The temperature was maintained at 0 °C and colorless product was obtained with yield of 68%. ¹H NMR (400 MHz, CDCl₃ + (CD₃)₂CO, 25 °C): δ (ppm) = 8.73 (d, 4H, ³J = 8.0 Hz, pyridinyl), 7.69 (d, 4H, ³J = 8.0 Hz, pyridinyl), 4.34 (s, 6H, NCH₃), 2.15 (m, 12H, PCH₂CH₃), 1.18 (m, 18H, PCH₂CH₃); ³¹P{¹H} NMR (CDCl₃, 121.5 MHz): δ 12.56 (*J*_{Pt-P} = 2250 Hz). ¹³C{¹H} NMR (75.5 MHz, CD₂Cl₂, 25 °C): δ (ppm) = 144.43, 144.13, 136.70, 128.53, 122.64, 119.45, 110.19, 47.21, 16.42, 8.07; ESI-MS *m/z*: 814.1 [M – OTf]¹⁺, 332.5 [M – 2OTf]²⁺, (M = C₃₀H₄₄F₆N₂O₆P₂PtS₂). IR (ATR, cm⁻¹) $\tilde{\nu}_{C\equiv C}$ = 2081. E. A. Pred.: C 37.4% H 4.6% N 2.9% Found: C 36.7%, H 4.6%, N 2.9%**



***trans*-[Pt(PEt₃)₂(C≡C-3-C₅H₄NCH₃)₂]**·2SO₃CF₃ 4-Me.** The temperature was maintained at 0 °C and colorless product was obtained with yield of 70%. ¹H NMR (300 MHz, CDCl₃ + (CD₃)₂CO, 25 °C): δ (ppm) = 8.84 (s, 2H, pyridinyl), 8.80 (d, 2H, ³J = 8.0 Hz, pyridinyl) 8.35 (d, 2H, ³J = 12.0 Hz, pyridinyl), 7.99 (t, 2H, ³J = 8.0 Hz, pyridinyl), 4.51 (s, 6H, NCH₃), 2.17 (m, 12H, PCH₂CH₃), 1.20 (m, 18H, PCH₂CH₃); ³¹P{¹H} NMR (CDCl₃ + (CD₃)₂CO, 121.5 MHz, 25 °C): δ (ppm) = 12.49 (*J*_{Pt-P} = 2282 Hz). ¹³C{¹H} NMR (100.6 MHz, CDCl₃ + (CD₃)₂CO, 25 °C): δ (ppm) = 146.22, 145.66, 141.16, 129.24, 127.64, 109.98, 103.20, 48.20, 16.32, 7.91; ESI-MS *m/z*: 814.1 [M – OTf]¹⁺, 332.5 [M – 2OTf]²⁺, (M = C₃₀H₄₄F₆N₂O₆P₂PtS₂). IR (ATR, cm⁻¹) $\tilde{\nu}_{C\equiv C}$ = 2106. E. A. Pred.: C 37.4% H 4.6% N 2.9% Found: C 37.5%, H 4.6%, N 2.9%**

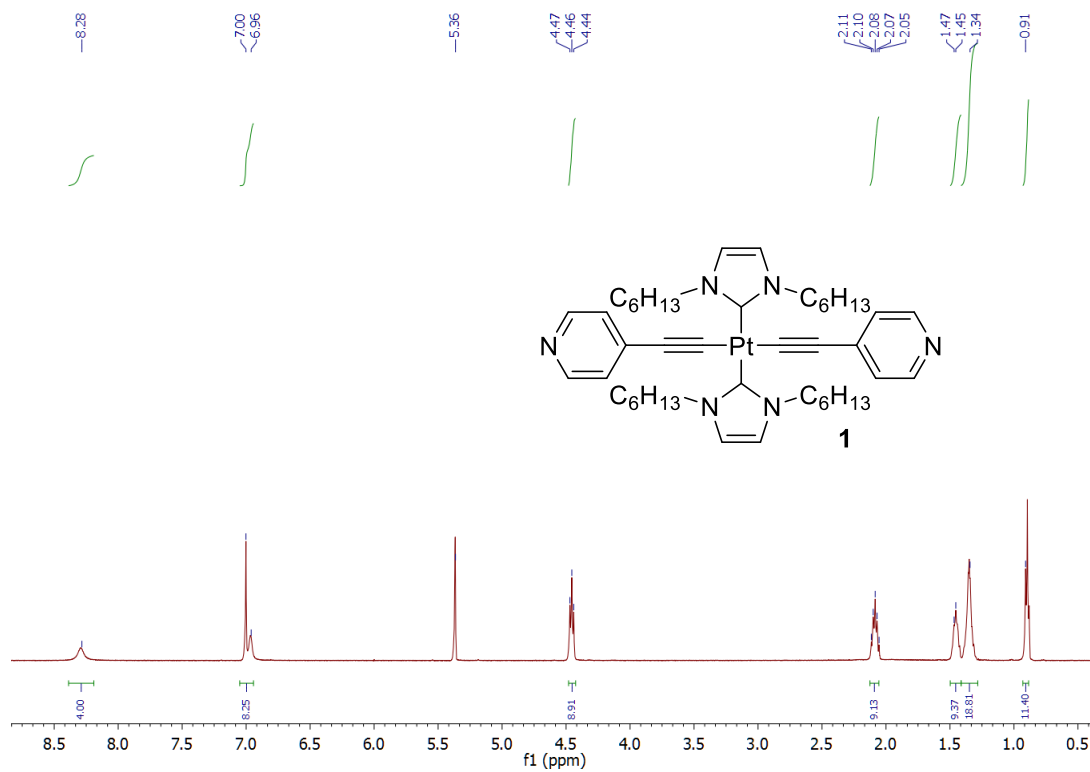


Figure S1. ¹H-NMR spectrum of **1** (CD₂Cl₂ at 25°C)

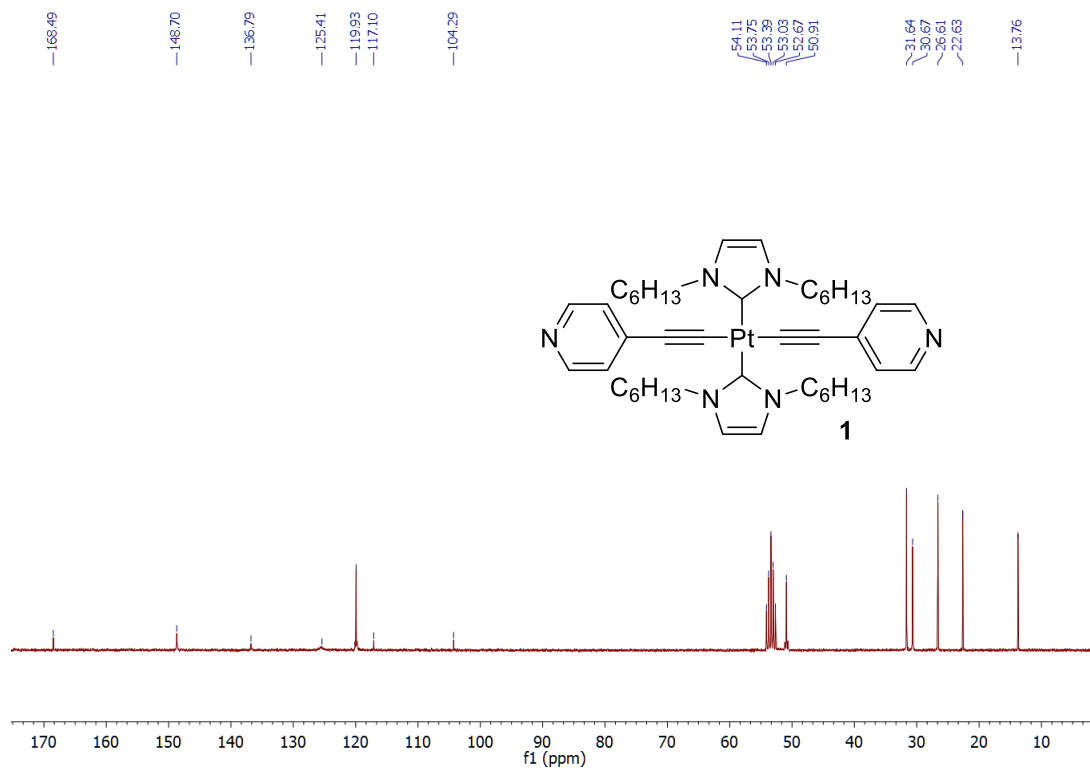


Figure S2. ¹³C-NMR spectrum of **1** (CD₂Cl₂ at 25°C)

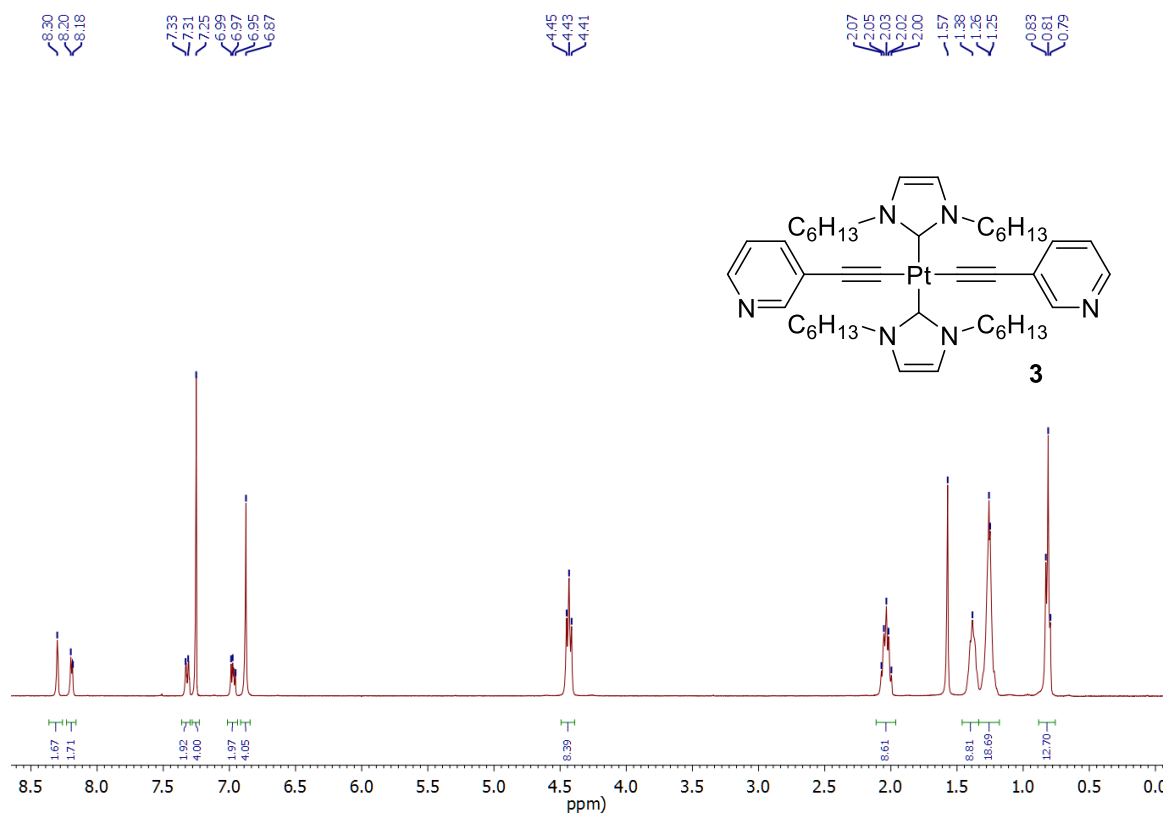
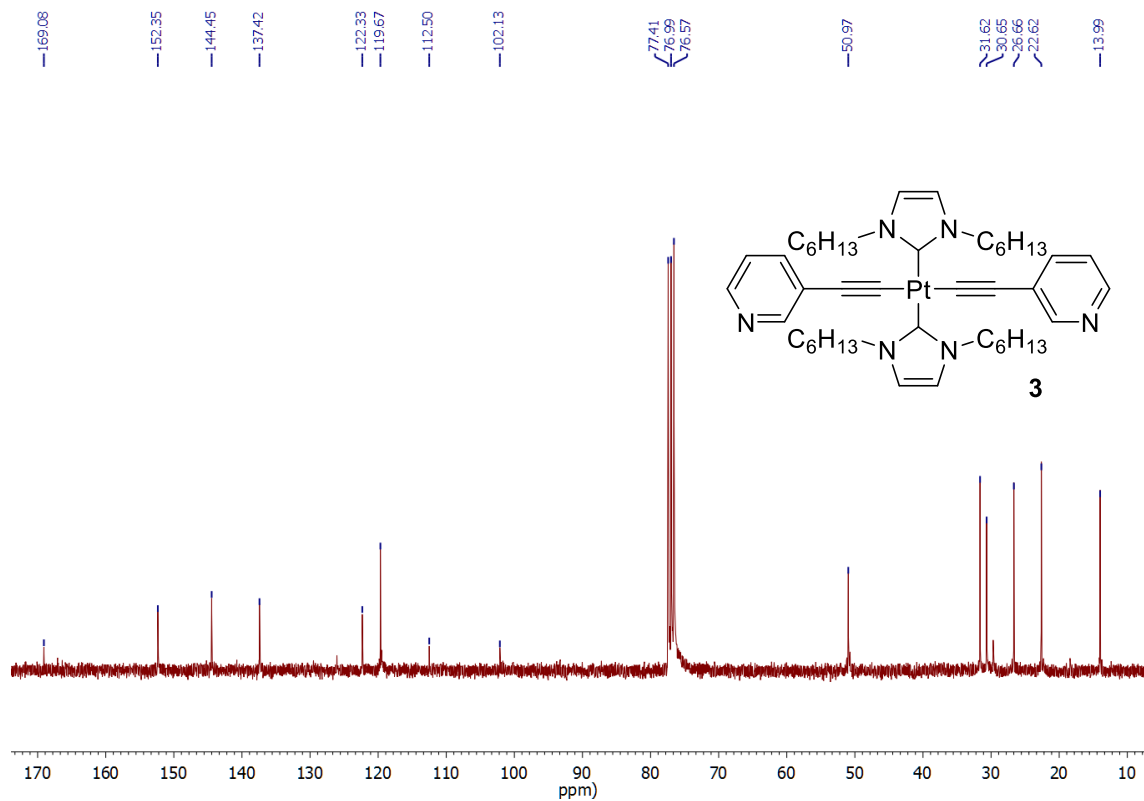


Figure S3. $^1\text{H-NMR}$ of **3** (CDCl_3 at 25°C)



Figure

S4. ¹³C-NMR of **3** (CDCl₃ at 25°C)

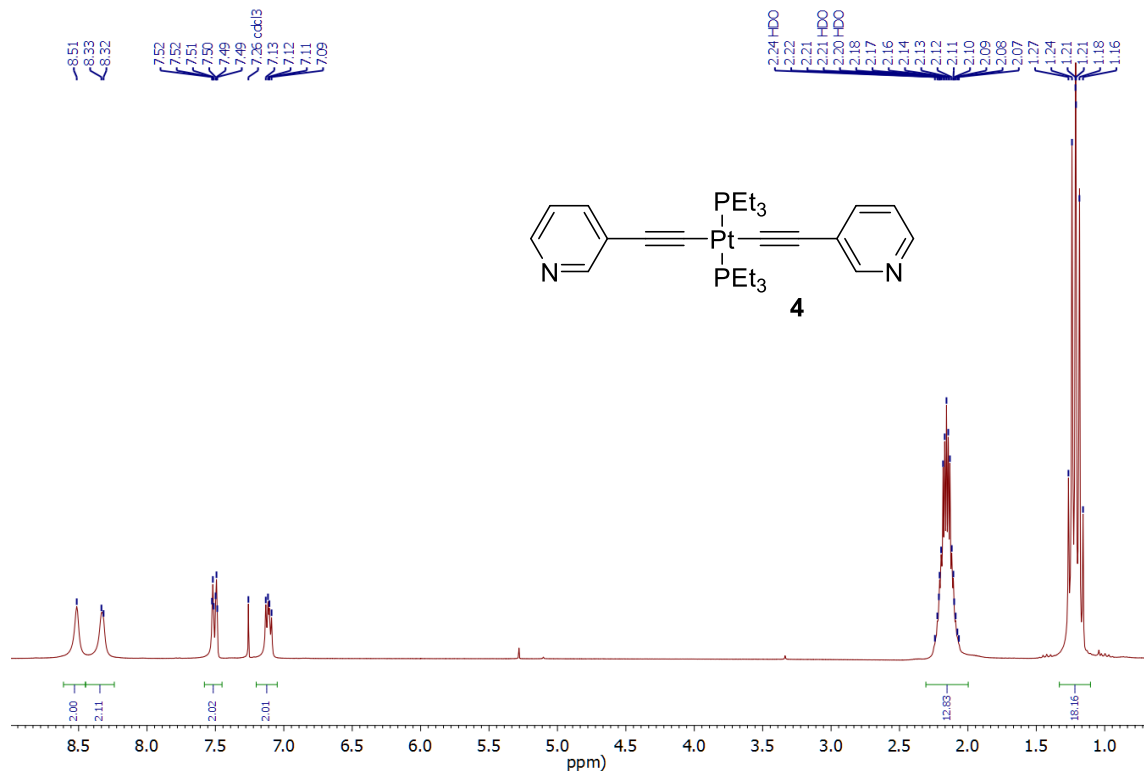
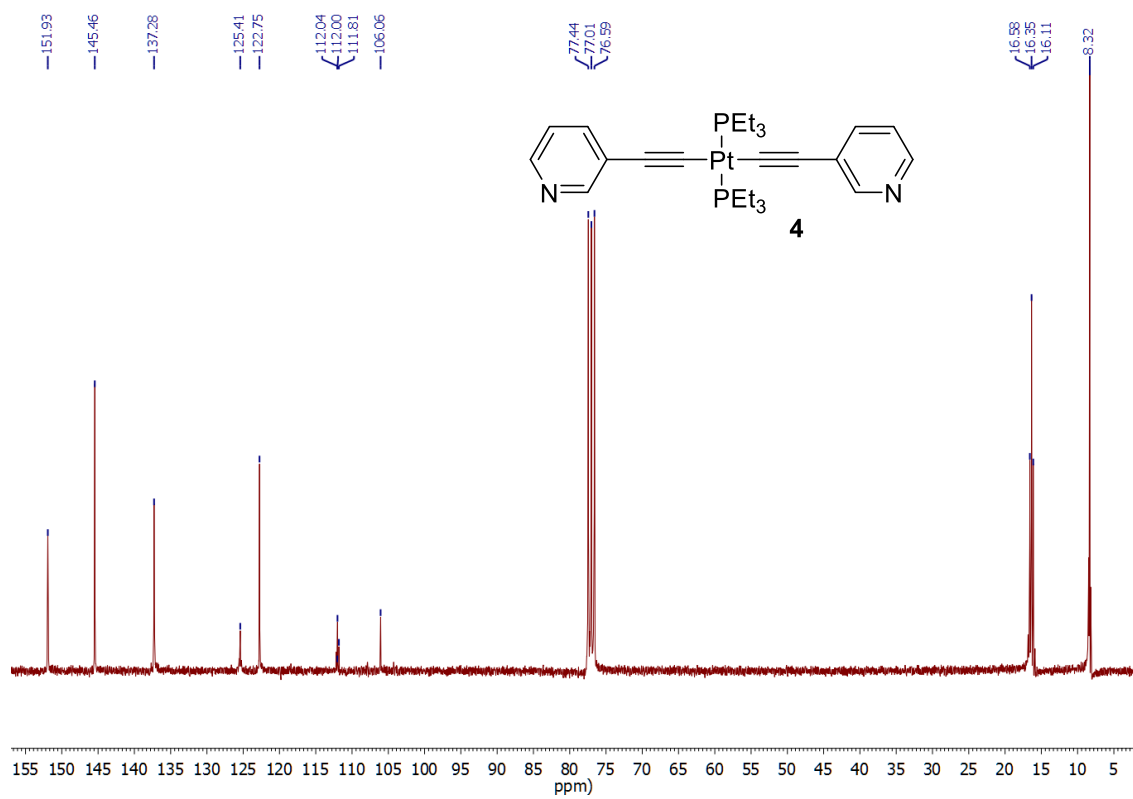


Figure S5. ¹H-NMR of **4** (CDCl₃ at 25°C)



Figure

S6. ^{13}C -NMR of **4** (CDCl_3 at 25°C)

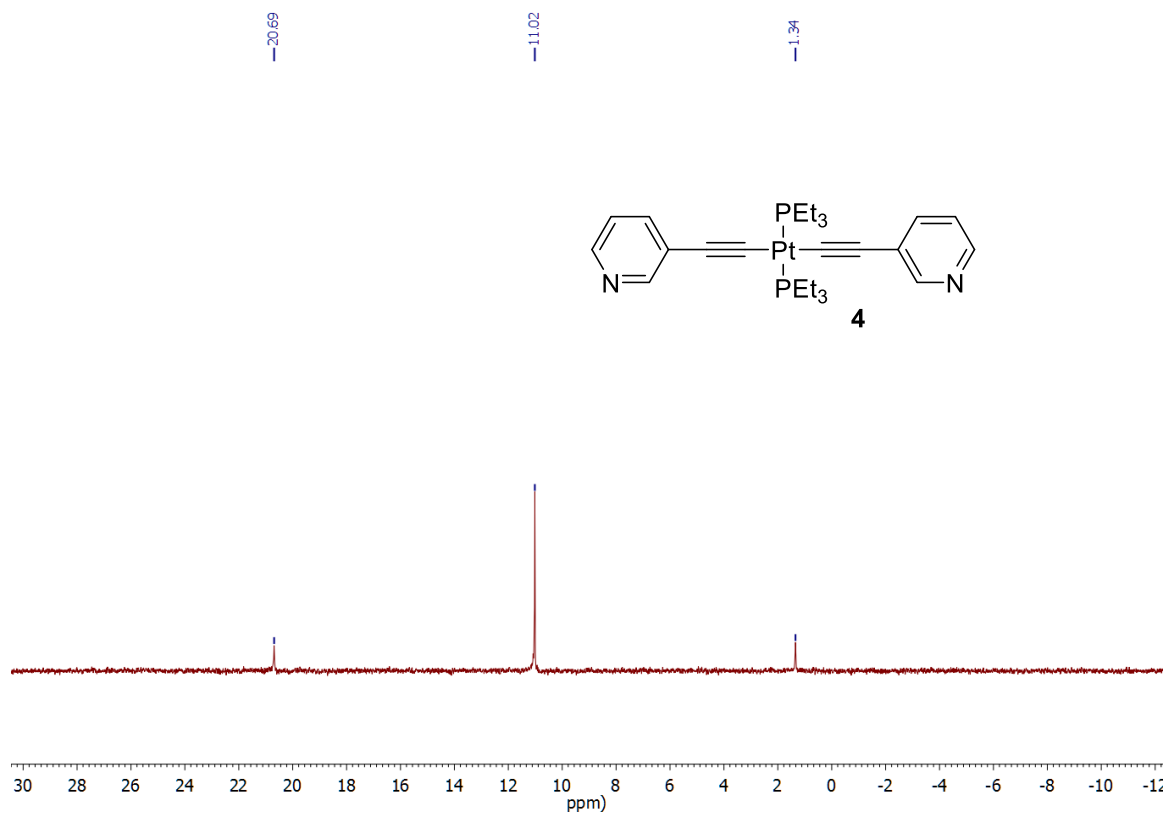
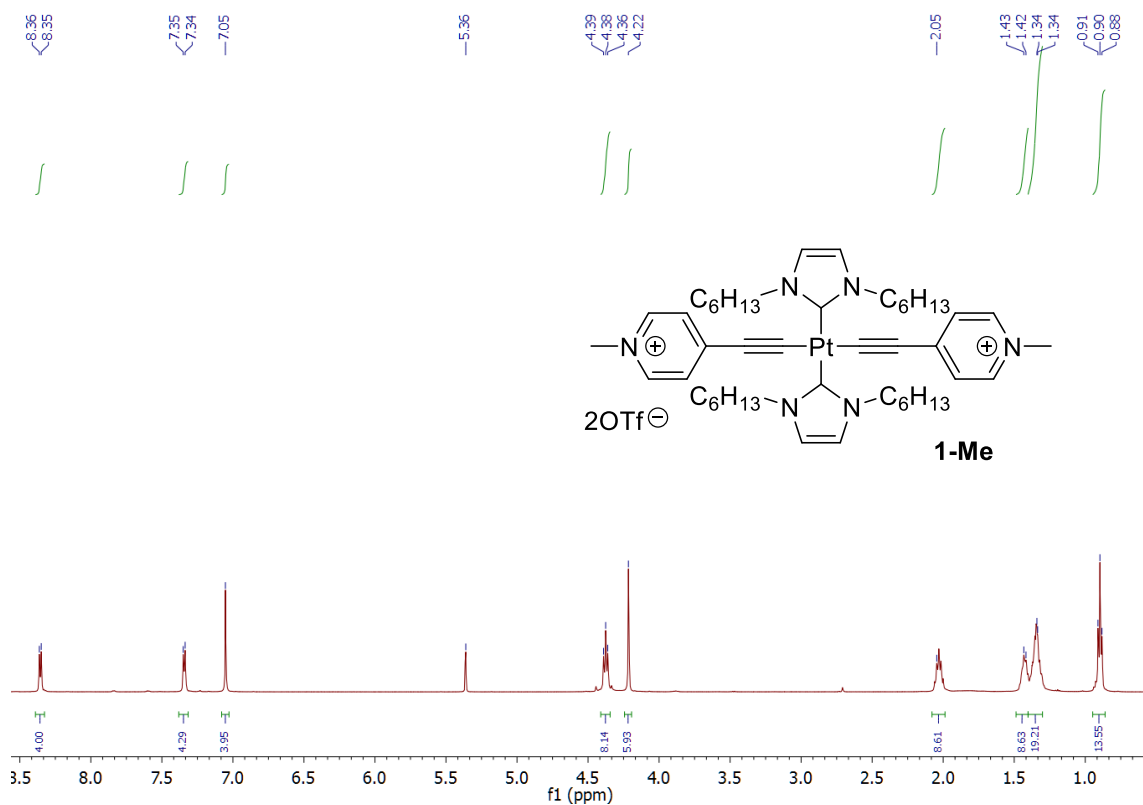
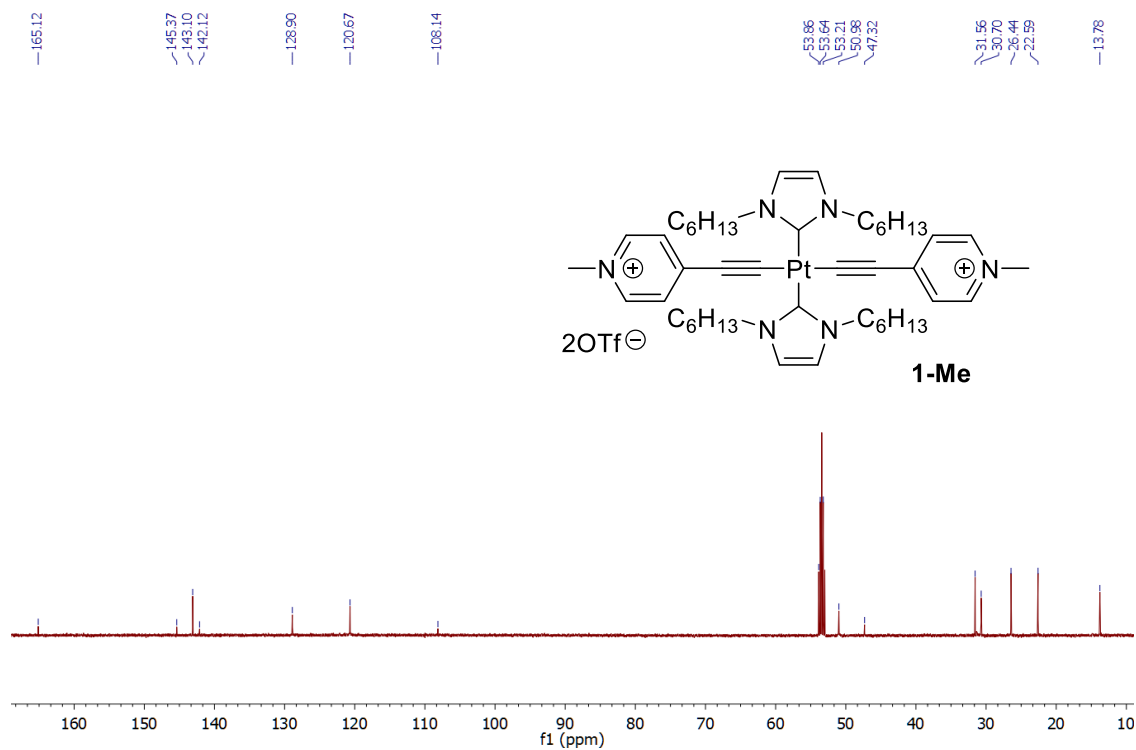


Figure S7. ^{31}P -NMR of **4** (CDCl_3 at 25°C)



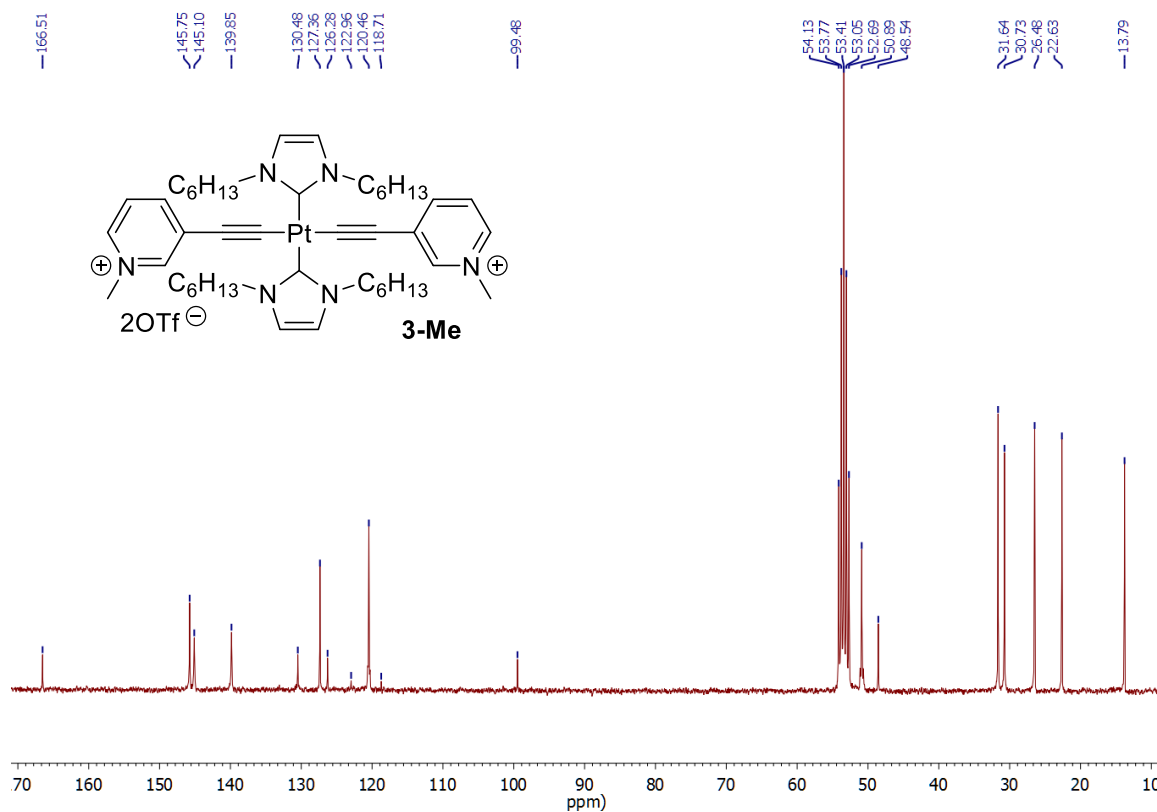
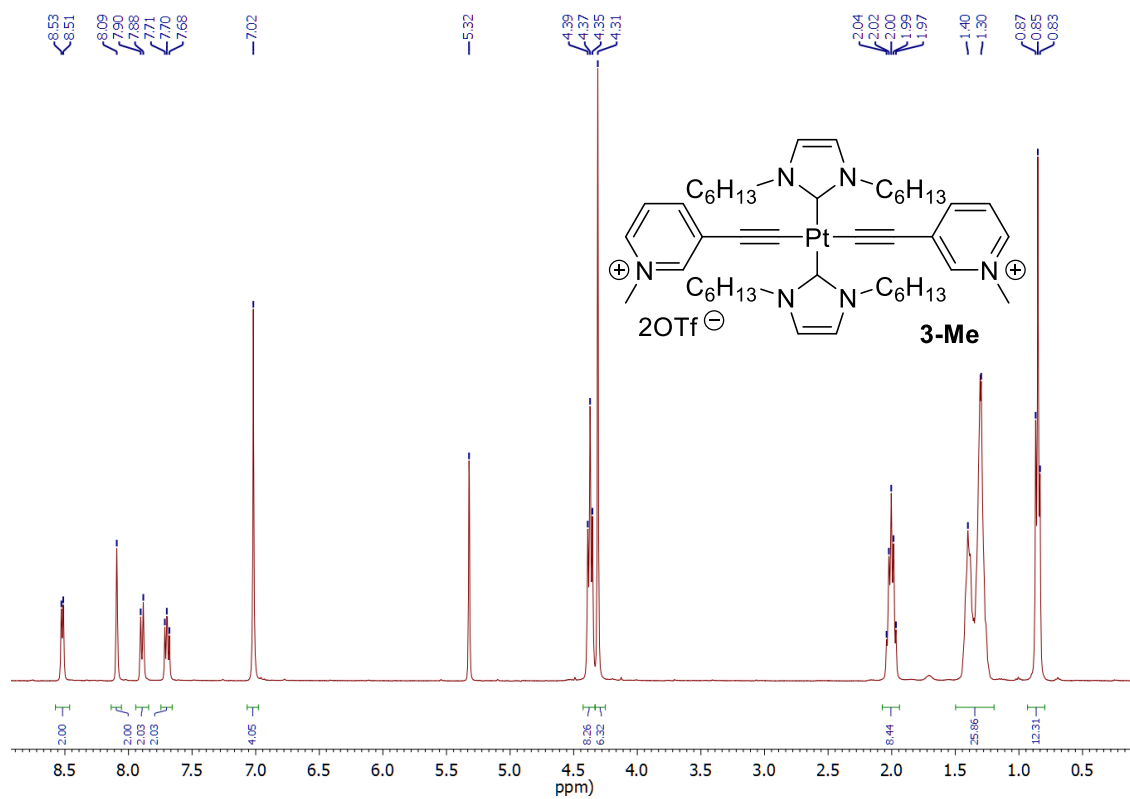
Figure

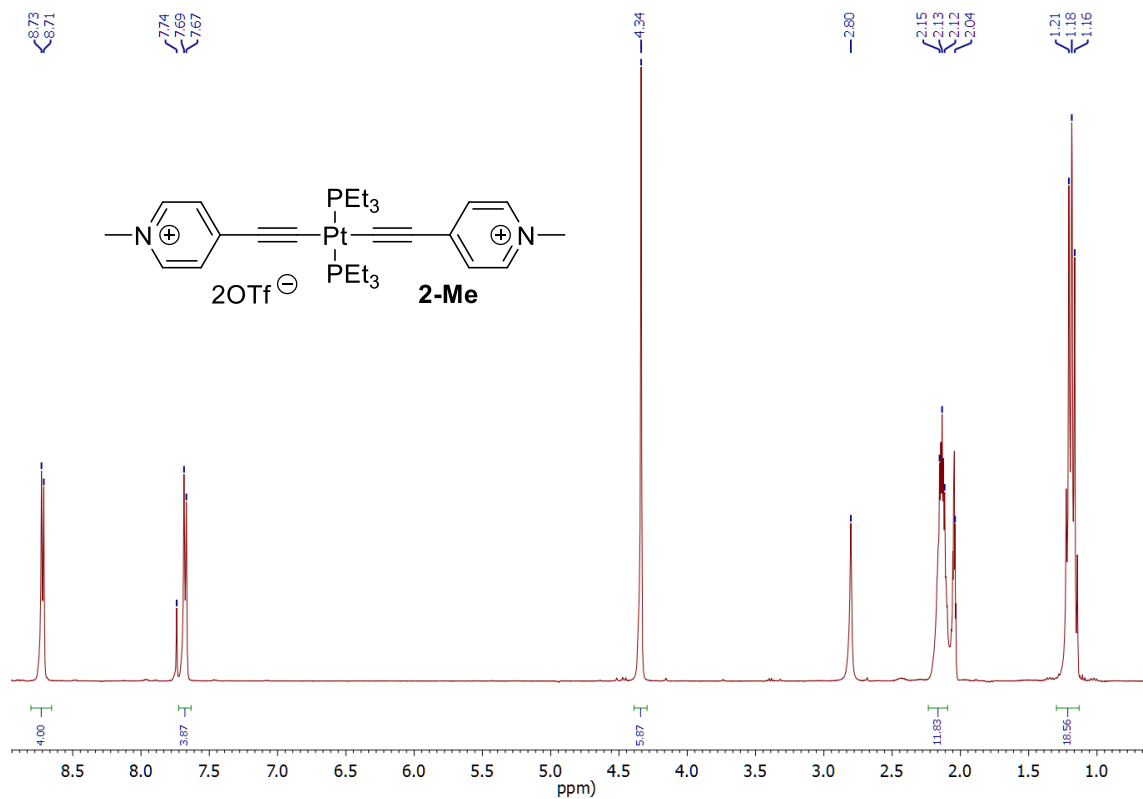
S8. ¹H-NMR of 1-Me (CD₂Cl₂ at 25°C)



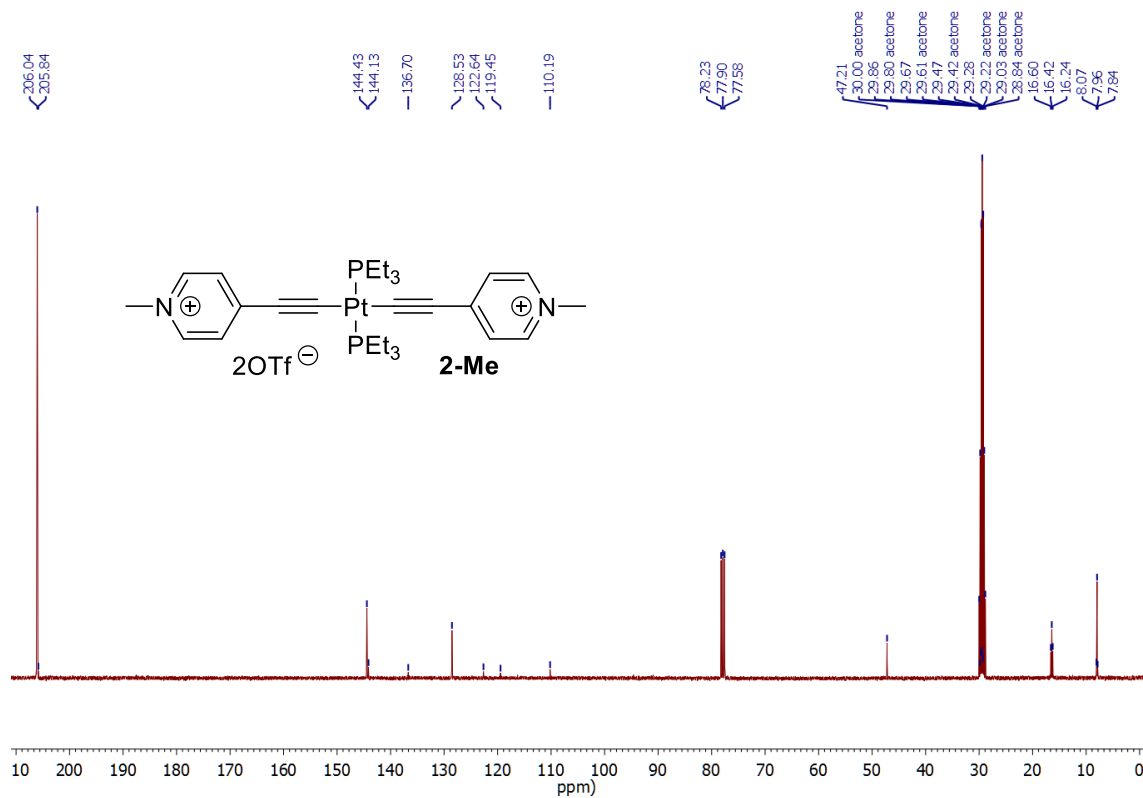
Figure

S9. ¹³C-NMR of 1-Me (CD₂Cl₂ at 25°C)





Figure



Figure

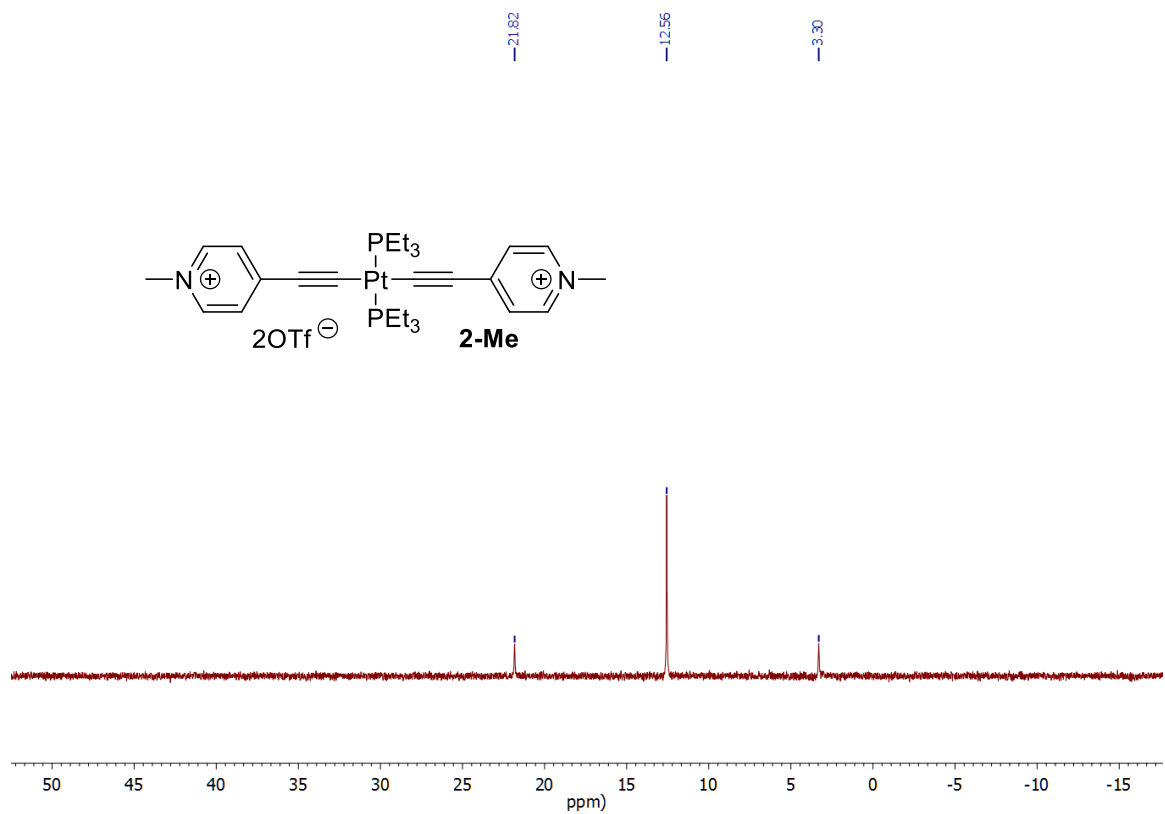


Figure S14. ³¹P-NMR of **2-Me** (CDCl₃ at 25°C)

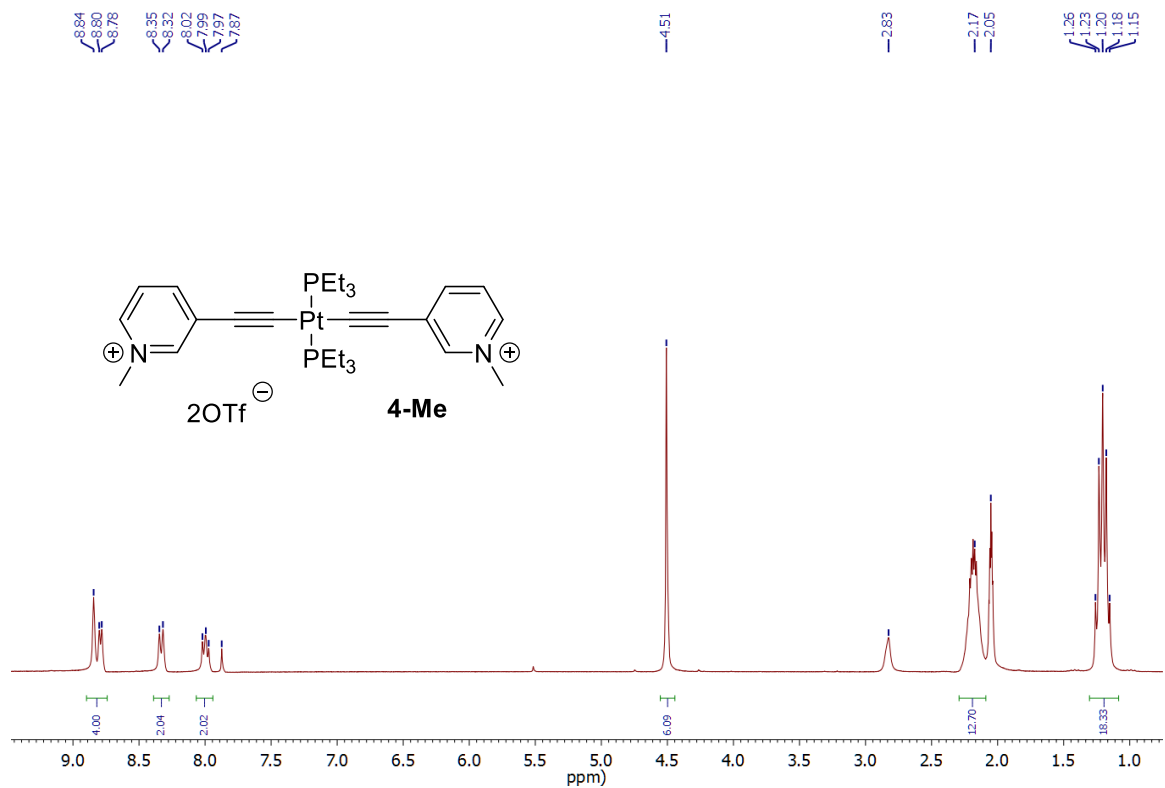
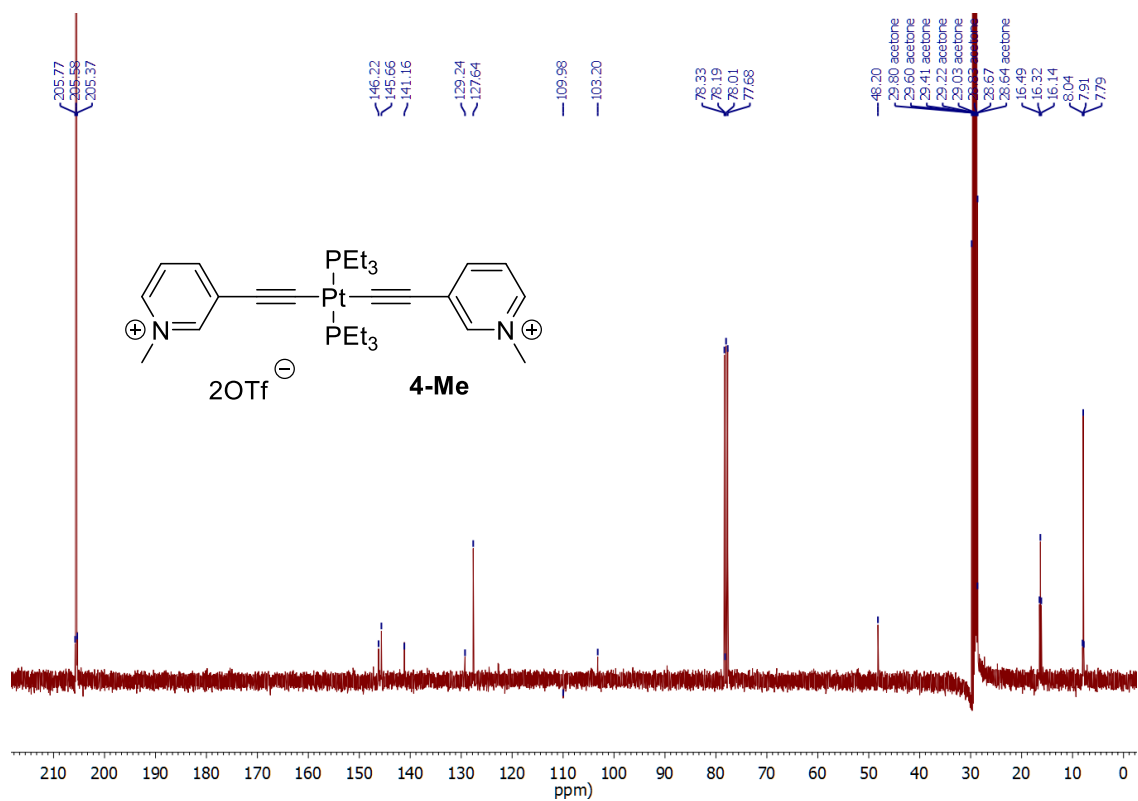


Figure S15. ¹H-NMR of **4-Me** (CDCl₃ + (CD₃)₂CO at 25°C)



Figure

S16. ^{13}C -NMR of **4-Me** ($\text{CDCl}_3 + (\text{CD}_3)_2\text{CO}$ at 25°C)

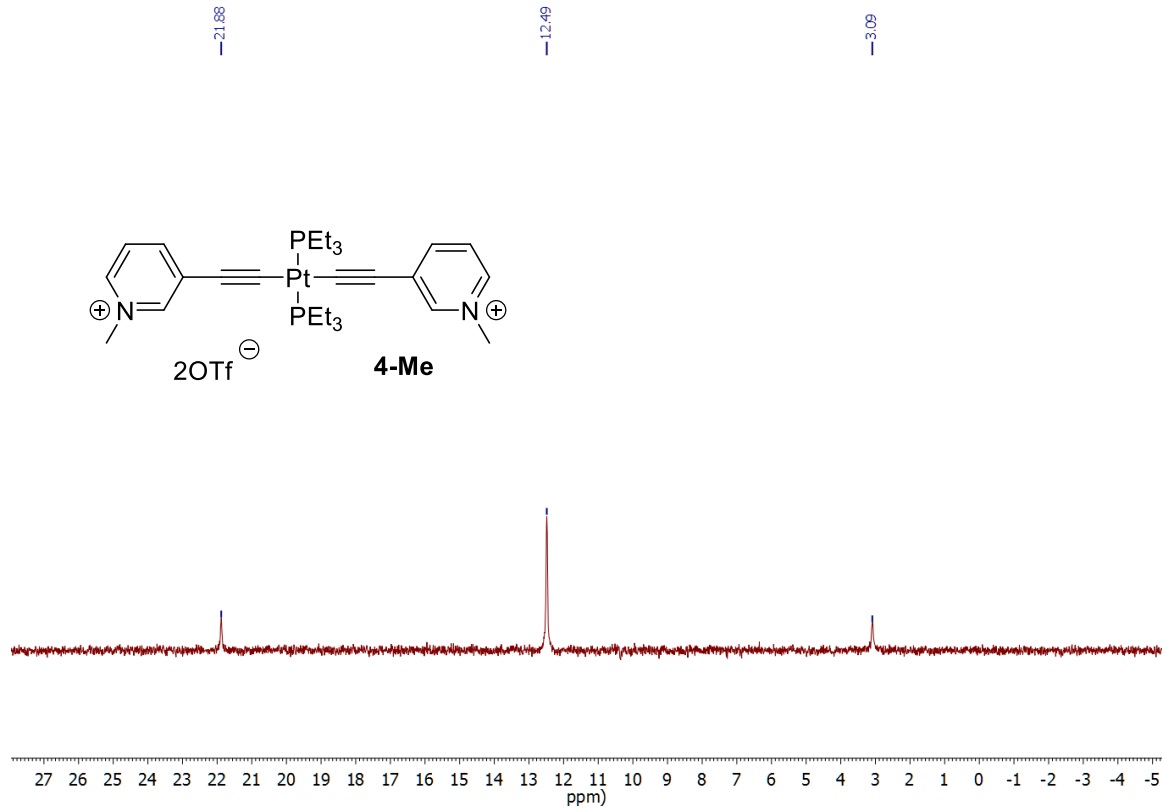


Figure S17. ^{31}P -NMR of **4-Me** (CDCl_3 and $(\text{CD}_3)_2\text{CO}$ at 25°C)

Photophysical Details

UV-vis absorption measurements were carried out on a Cary 8454 UV-Vis Diode Array System. Measurements were made in duplicate, with each sample solution diluted five times for a total of ten measurements. Emission spectra were acquired on Horiba Fluoromax-4 spectrometer using 450 W xenon lamp. Slit widths were set wide enough to observe spectra without saturating the PMT detector, usually between 1 to 10 nm bandpass. All samples for emission spectra were prepared in N₂-filled glove boxes in 1 cm path length cuvettes. Absolute luminescent quantum yields were measured using a Horiba Quanta-φ integrating light sphere. Excitation wavelengths were set to the lowest energy absorption maxima, but in no case was it set at a higher energy than 330 nm. Both excitation and emission slit widths were set to 3 nm, as per manufacturer instructions. Calculations of quantum yields were performed using the FluorEssence software package, version 3.5.8.63. Lifetimes were measured using the Horiba DeltaTime Time-correlated Single Photon Counting (TCSPC) system with the NanoLED-350 350 nm diode source or SpectraLED-355 355 nm diode source, as appropriate. Data analysis was performed using the Decay Analysis Software (DAS6), version 6.8.10.

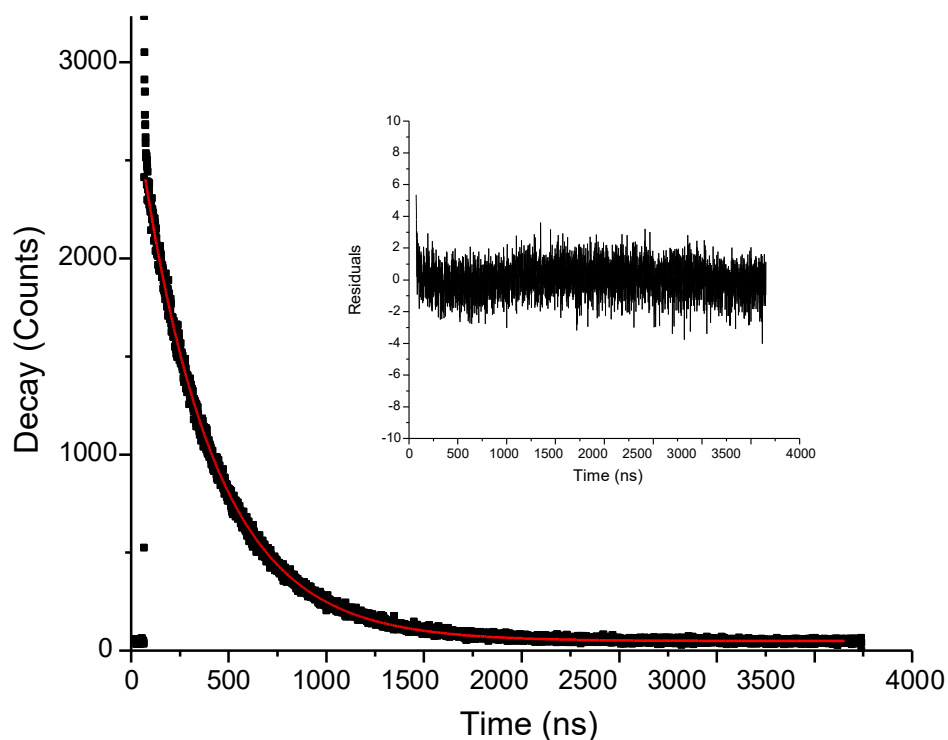


Figure S18. Decay trace (black) and fit line (red) for **1** as measured at 434 nm. Monoexponential fit ($\chi = 1.07$) Inset: Residual Plot.

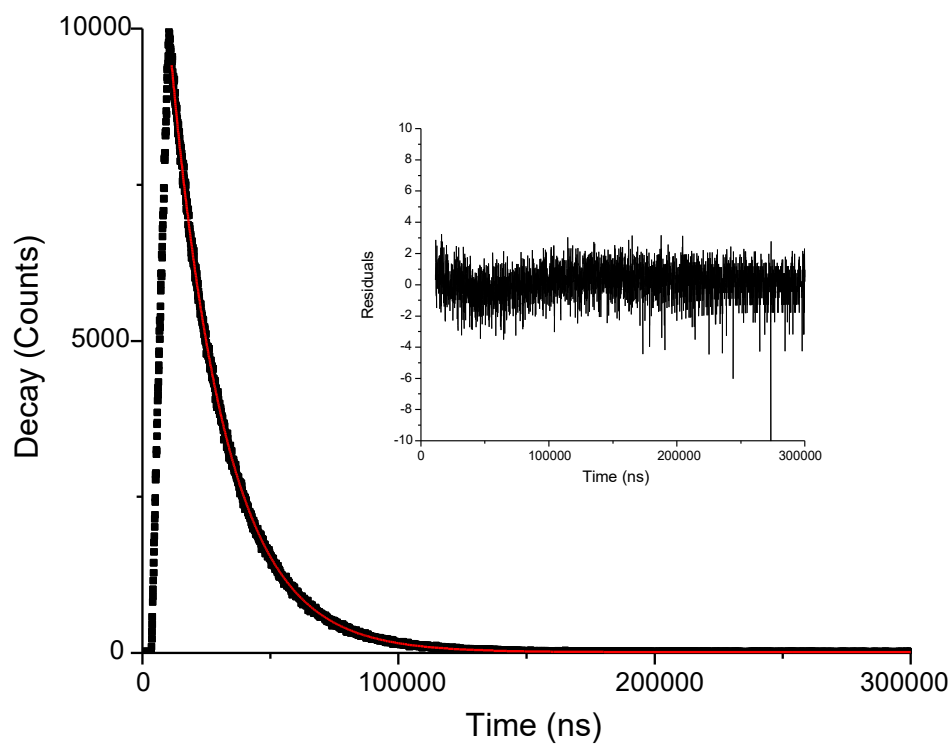


Figure S19. Decay trace (black) and fit line (red) for **1-Me** as measured at 512 nm. Monoexponential fit ($\chi = 1.18$) Inset: Residual Plot.

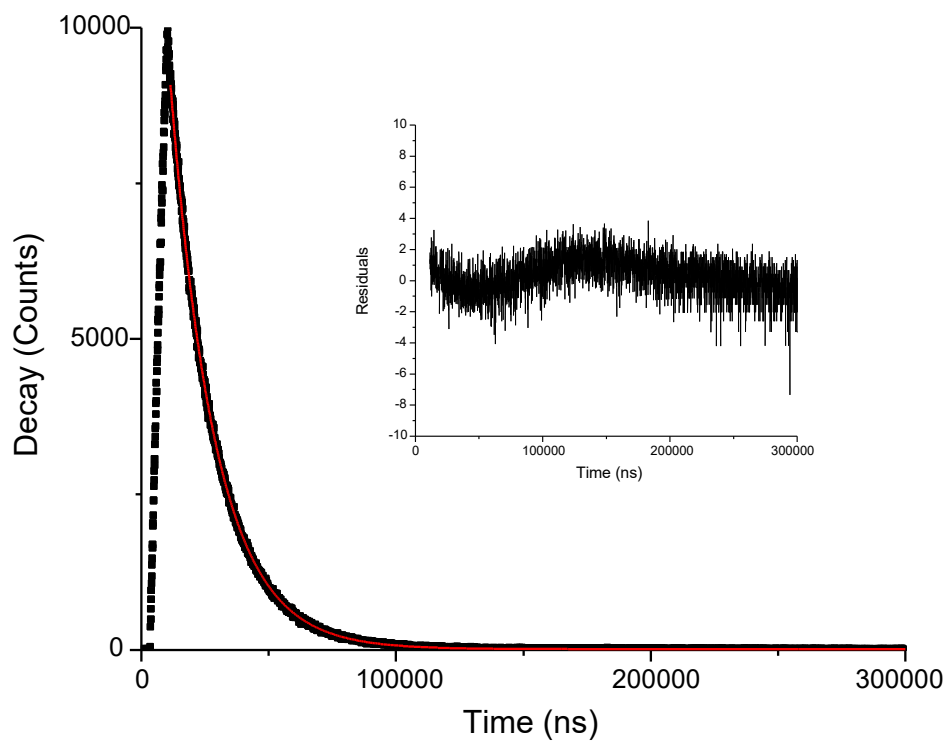


Figure S20. Decay trace (black) and fit line (red) for **3** as measured at 448 nm. Monoexponential fit ($\chi = 1.57$) Inset: Residual Plot.

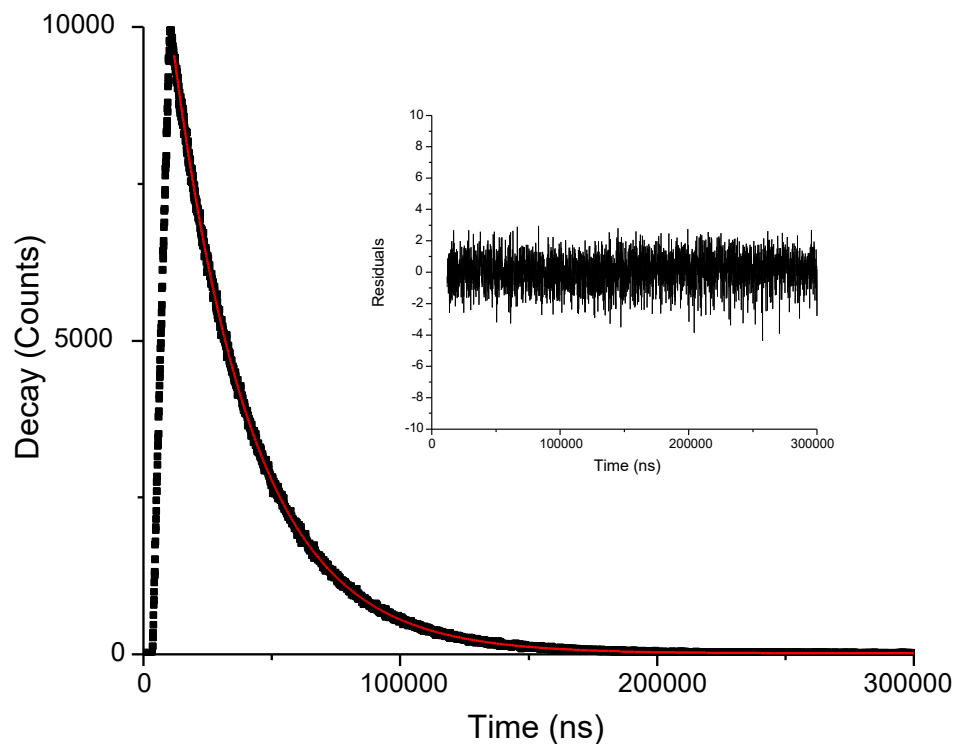


Figure S21. Decay trace (black) and fit line (red) for **3-Me** as measured at 560 nm. Monoexponential fit ($\chi = 1.09$) Inset: Residual Plot.

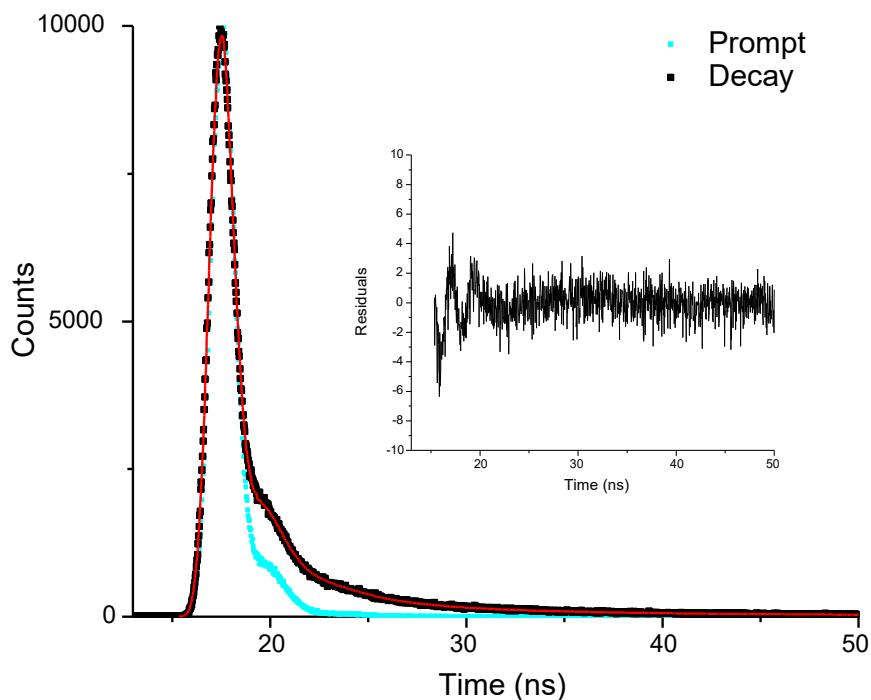


Figure S22. Decay trace (black) and fit line (red) for **2** as measured at 400 nm. Triexponential fit (instrument response from solvent Raman scatter, fluorescence, and phosphorescence, $\chi = 1.31$) Inset: Residual Plot.

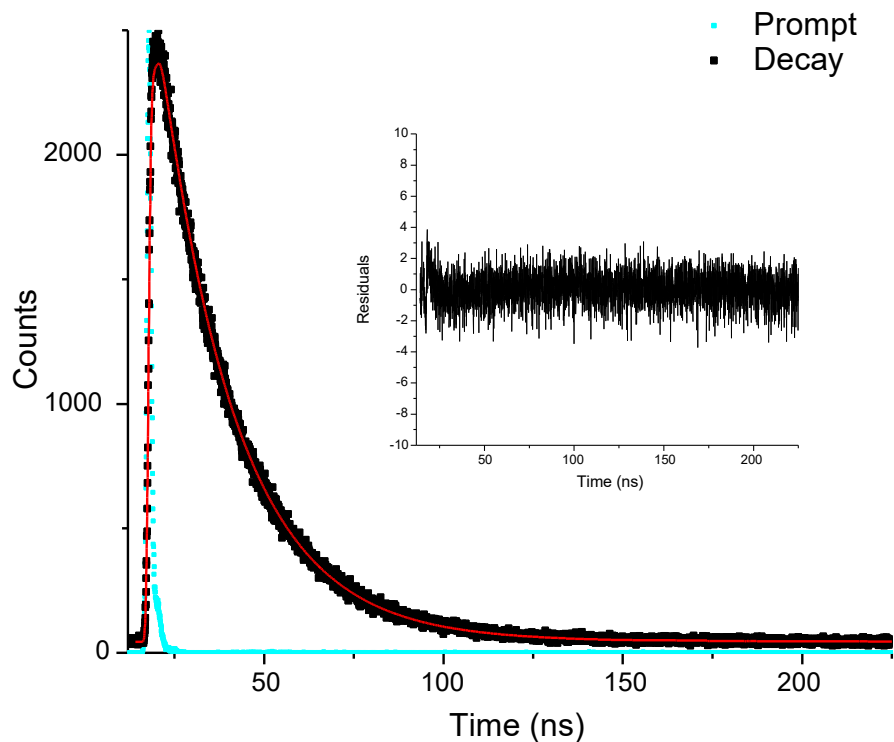


Figure S23. Decay trace (black) and fit line (red) for **2-Me** as measured at 493 nm. Monoexponential fit ($\chi = 1.06$) Inset: Residual Plot.

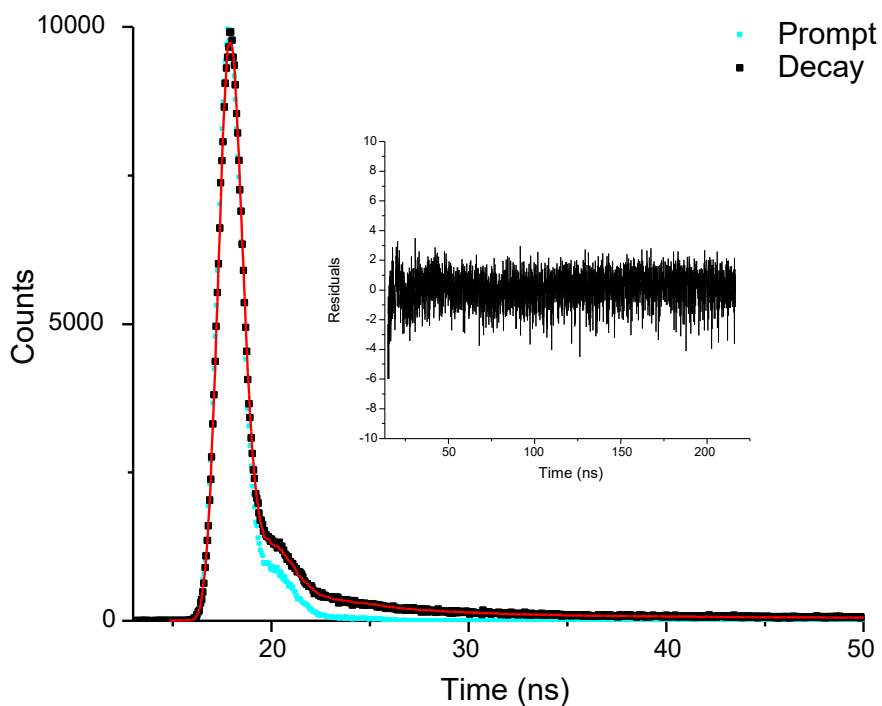


Figure S24. Decay trace (black) and fit line (red) for **4** as measured at 390 nm. Triexponential fit (instrument response from solvent Raman scatter, fluorescence, and phosphorescence, $\chi = 1.18$) Inset: Residual Plot.

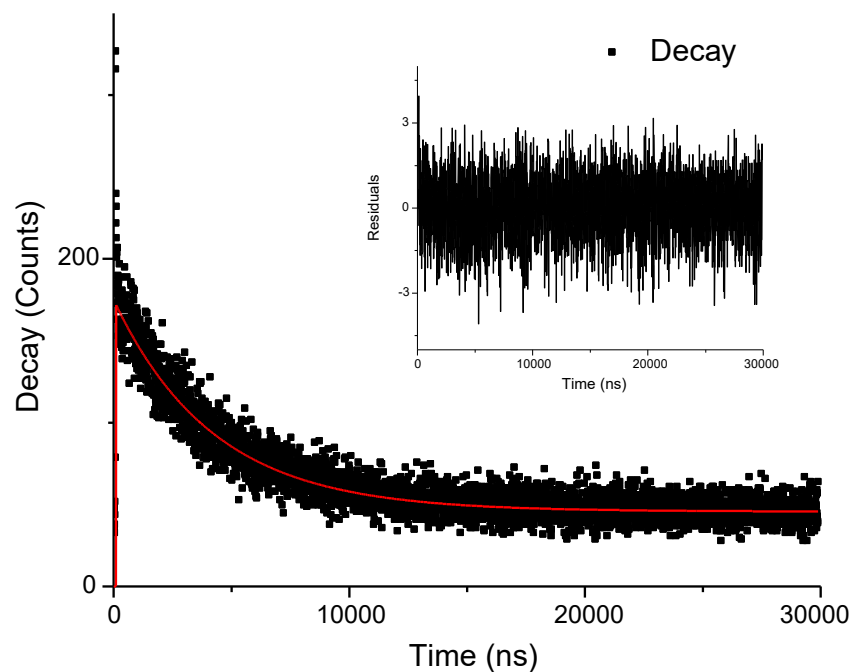


Figure S25. Decay trace (black) and fit line (red) for **4-Me** as measured at 525 nm. Monoexponential fit ($\chi = 1.08$) Inset: Residual Plot.

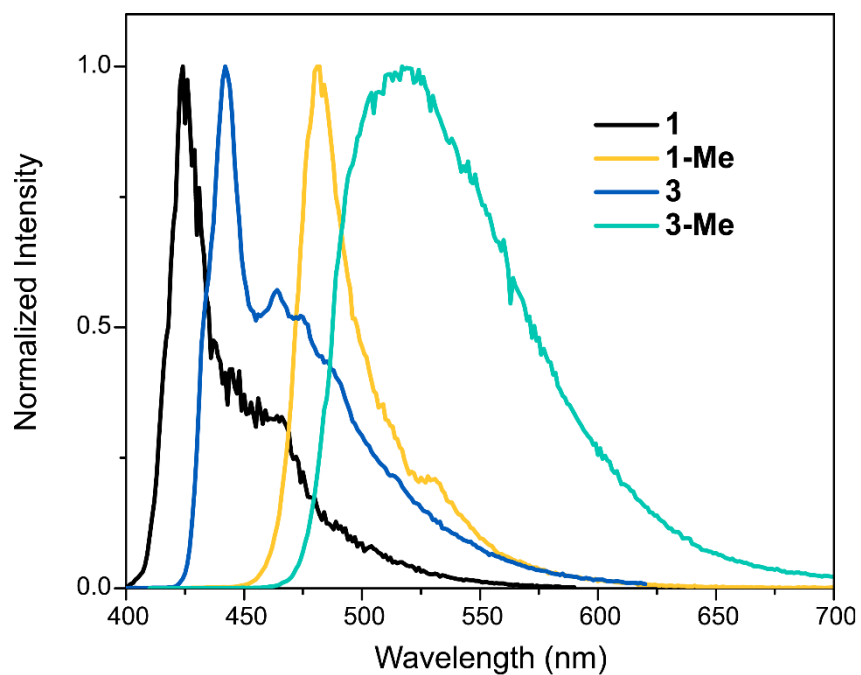


Figure S26. Emission spectra of **1**, **1-Me**, **3**, and **3-Me** in THF at 77 K

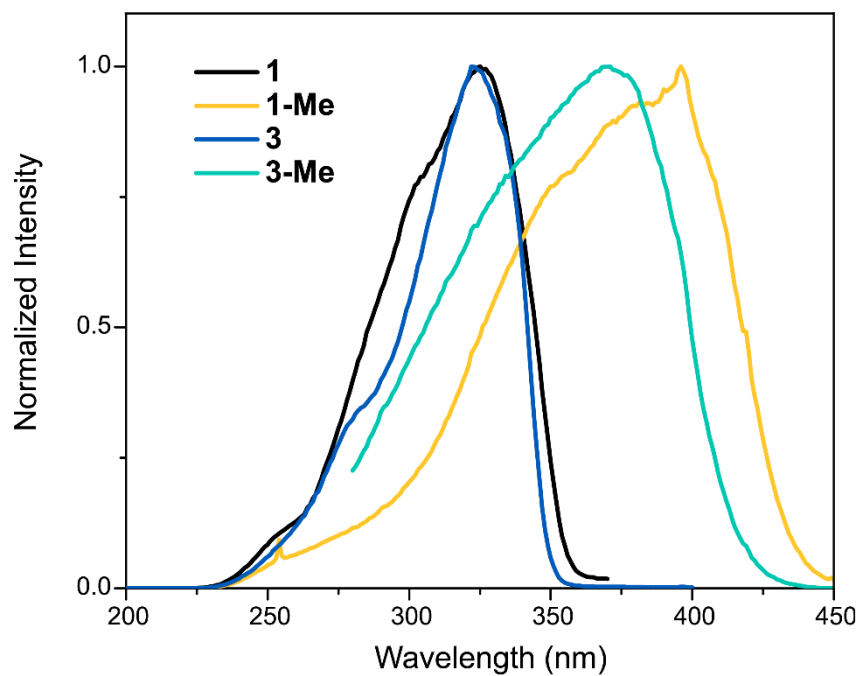


Figure S27. Excitation spectra of **1**, **1-Me**, **3**, and **3-Me** in THF. Emission monochromator set at the emission maximum of each compound.

Computational Details

All calculations and geometry optimizations were performed at the B3LYP level of theory, using the LANL2DZ basis set for platinum and 6-31G(d,p) for all other elements. All alkyl groups were modeled as methyl groups. Singlet optimizations were calculated using the restricted formalism. The characterization of absorptions bands was performed with the aid of time-dependent density functional theory (TD-DFT). The first 50 transitions were analyzed (CI expressed as absolute value in tables below). HOMO is represented as “H” and LUMO as “L” in the tables and figures below. Triplet excited state geometries were obtained by following method. A TD-DFT calculation was performed to find the first 50 singlet-to-triplet transitions. These transitions were then analyzed to determine which best corresponded to the high oscillator strength transitions found in the original singlet-to-singlet TD-DFT. The criteria used for analysis was that the orbitals the transition was from and to matched reasonably well, that weights of multi-orbital transitions matched reasonably well, and that the singlet-to-triplet transition occurred at a lower energy than the corresponding singlet-to-singlet transition. This was performed for the lowest energy singlet-to-singlet transition with significant oscillator strength (i.e. the lowest energy observable absorptive transition) for each molecule. The excited state corresponding to the selected singlet-to-triplet transition was then geometry optimized. To characterize the shift in electron density, a natural population analysis was performed for both the ground and excited states of each molecule using Natural Bond Orbital (NBO) version 3.1. This, along with the nature of the highest singly occupied molecular orbital (SOMO), was used to characterize emission bands. All calculations were performed using Gaussian 09 software package⁴.

Table S1. Calculated electronic transition energies of the low-lying singlet excited states of **1**

electronic transition	absorption wavelength/nm (energy/eV)	f	contribution	CI
$S_0 \rightarrow S_1$	317 (3.9136)	0.0000	H – 7 \rightarrow L + 1	0.13907
			H – 1 \rightarrow L	0.68686
$S_0 \rightarrow S_2$	303 (4.0891)	0.0000	H – 7 \rightarrow L	0.18611
			H – 1 \rightarrow L + 1	0.67305
$S_0 \rightarrow S_3$	297 (4.1730)	0.0103	H \rightarrow L + 2	0.70135
$S_0 \rightarrow S_4$	296 (4.1913)	0.0465	H – 1 \rightarrow L + 2	0.57608
			H \rightarrow L	0.39725
$S_0 \rightarrow S_5$	287 (4.3169)	0.8600	H – 1 \rightarrow L + 2	0.39696
			H \rightarrow L	0.57138

$S_0 \rightarrow S_6$	272 (4.5519)	0.0000	$H - 2 \rightarrow L$	0.13976
			$H \rightarrow L + 1$	0.68328
$S_0 \rightarrow S_7$	266 (4.6632)	0.0000	$H - 2 \rightarrow L + 2$	0.70068
$S_0 \rightarrow S_8$	261 (4.7436)	0.0000	$H - 7 \rightarrow L$	0.15684
			$H - 6 \rightarrow L + 1$	0.44217
			$H - 5 \rightarrow L$	0.51629
$S_0 \rightarrow S_9$	261 (4.7437)	0.0050	$H - 7 \rightarrow L + 1$	0.13128
			$H - 6 \rightarrow L$	0.53169
			$H - 5 \rightarrow L + 1$	0.42373
$S_0 \rightarrow S_{10}$	258 (4.8075)	0.0000	$H - 2 \rightarrow L$	0.66878
			$H \rightarrow L + 1$	0.10887

Table S2. Singlet to Triplet Transition Selected to Optimize for **1**

Singlet Transition Modeled	Triplet Transition Selected	Absorption wavelength (nm)	Contribution	CI
5	8	303	$H - 4 \rightarrow L + 2$	0.10551
			$H - 1 \rightarrow L$	0.11128
			$H \rightarrow L + 2$	0.67751

Table S3. Ligand and Functional Group Contributions to the Ground State Orbitals of **1**

Orbitals:	H - 4	H - 1	H	L	L + 2
Platinum Contribution	33.5%	41.5%	26.7%	1.9%	20.9%
Carbene Contribution	61.9%	5.0%	4.0%	4.7%	63.4%
Ethynyl Contribution	2.4%	44.7%	42.6%	15.1%	12.0%
Pyridine Contribution	2.2%	8.9%	26.7%	78.3%	3.7%

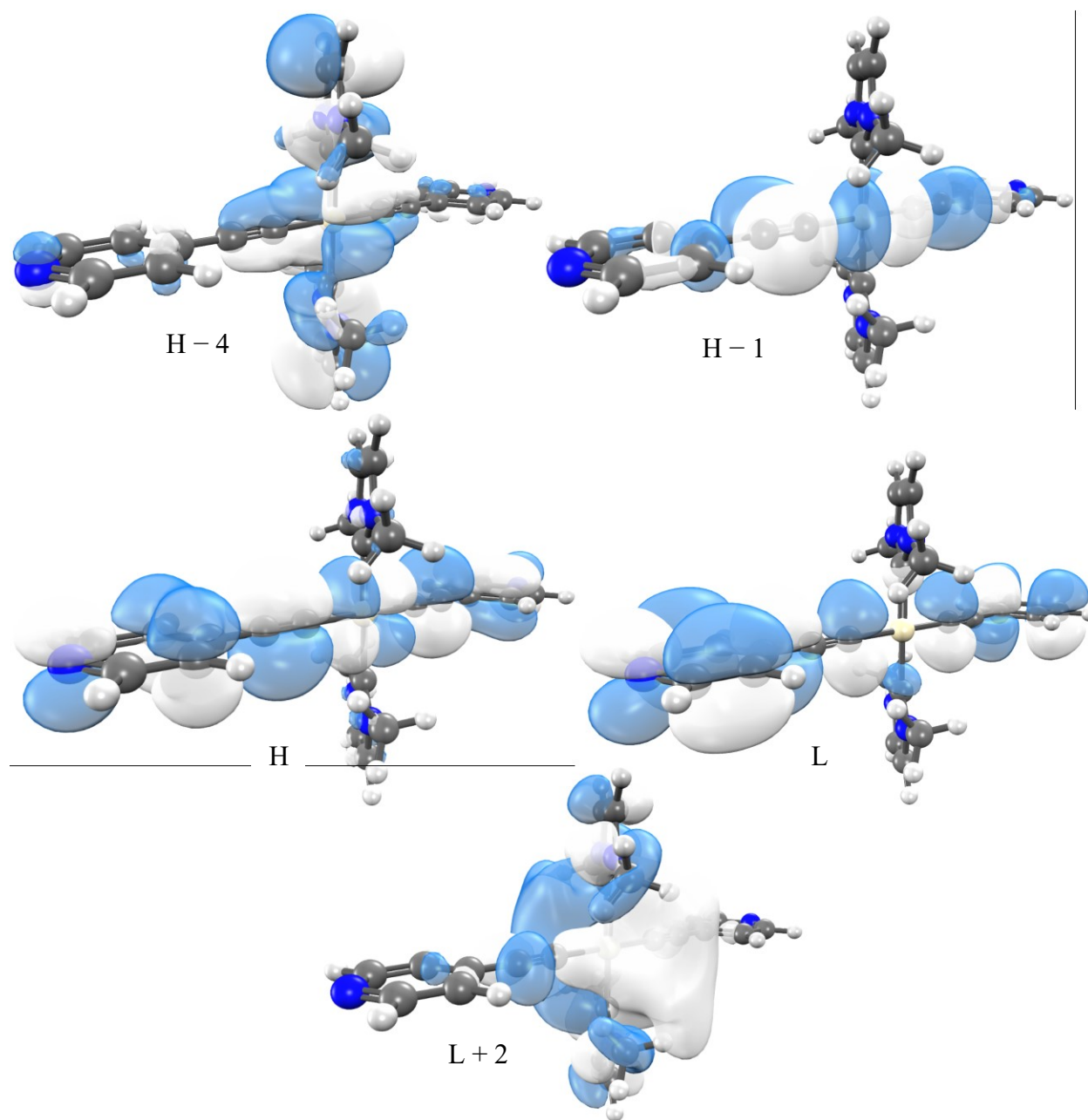


Figure S28. Relevant frontier orbitals for **1**, plotted with an isovalue of 0.04.

Table S4. Natural Population Analysis of **1** in both the ground and excited state.

	Charge in Ground State	Charge in Excited State	Electrons Gained
Platinum	-0.01	-0.04	+0.03
Ethynyl Left	-0.35	-0.20	-0.15
Pyridyl Left	-0.10	-0.25	+0.15
Ethynyl Right	-0.35	-0.34	-0.01
Pyridyl Right	-0.10	-0.10	0.00
NHC Top	0.46	0.47	-0.01
NHC Bottom	0.46	0.47	-0.01

Table S5. Calculated electronic transition energies of the low-lying singlet excited states of **1-Me**

electronic transition	absorption wavelength/nm (energy/eV)	f	contribution	CI
$S_0 \rightarrow S_1$	458 (2.7072)	0.0000	H - 6 \rightarrow L + 1	0.13539
			H - 5 \rightarrow L	0.12023
			H - 3 \rightarrow L + 1	0.10025
			H - 1 \rightarrow L + 1	0.1511
			H \rightarrow L	0.65629
$S_0 \rightarrow S_2$	449 (2.7594)	0.0285	H - 6 \rightarrow L	0.16109
			H - 3 \rightarrow L	0.10677
			H - 1 \rightarrow L	0.20306
			H \rightarrow L + 1	0.63916
$S_0 \rightarrow S_3$	398 (3.1148)	0.3597	H - 3 \rightarrow L	0.14017
			H - 1 \rightarrow L	0.66735
			H \rightarrow L + 1	0.17822
$S_0 \rightarrow S_4$	384 (3.2313)	0.0000	H - 3 \rightarrow L + 1	0.1814
			H - 1 \rightarrow L + 1	0.66548
			H \rightarrow L	0.10733
$S_0 \rightarrow S_5$	374 (3.3159)	0.0000	H - 4 \rightarrow L	0.70517
$S_0 \rightarrow S_6$	366 (3.3898)	0.0012	H - 4 \rightarrow L + 1	0.7045
$S_0 \rightarrow S_7$	362 (3.4245)	0.0000	H - 2 \rightarrow L	0.70455
$S_0 \rightarrow S_8$	354 (3.5043)	0.0000	H - 2 \rightarrow L + 1	0.70442
$S_0 \rightarrow S_9$	347 (3.5696)	0.7727	H - 6 \rightarrow L	0.12252
			H - 3 \rightarrow L	0.6642
			H \rightarrow L + 1	0.17492
			H - 6 \rightarrow L + 1	0.11312
$S_0 \rightarrow S_{10}$	337 (3.6826)	0.0000	H - 5 \rightarrow L	0.22675
			H - 3 \rightarrow L + 1	0.63693
			H - 1 \rightarrow L + 1	0.11823
			H \rightarrow L	0.10688

Table S6. Singlet to Triplet Transition Selected to Optimize for **1-Me**

Singlet Transition Modeled	Triplet Transition Selected	Absorption wavelength (nm)	Contribution	CI
3	1	522	H - 6 → L	0.13337
			H - 5 → L + 1	0.29725
			H - 3 → L	0.31368
			H - 1 → L	0.39006
			H → L + 1	0.36714

Table S7. Ligand and Functional Group Contributions to the Ground State Orbitals of **1-Me**

Orbitals:	H - 6	H - 5	H - 3	H - 1	H	L	L + 1
Platinum Contribution	2.6%	1.8%	2.0%	34.2%	47.0%	1.7%	4.3%
Carbene Contribution	1.4%	23.8%	44.5%	41.6%	0.8%	2.6%	1.1%
Ethynyl Contribution	77.4%	47.8%	34.2%	14.0%	39.2%	12.5%	12.6%
Pyridine Contribution	18.5%	26.6%	19.3%	10.2%	13.1%	83.3%	82.0%

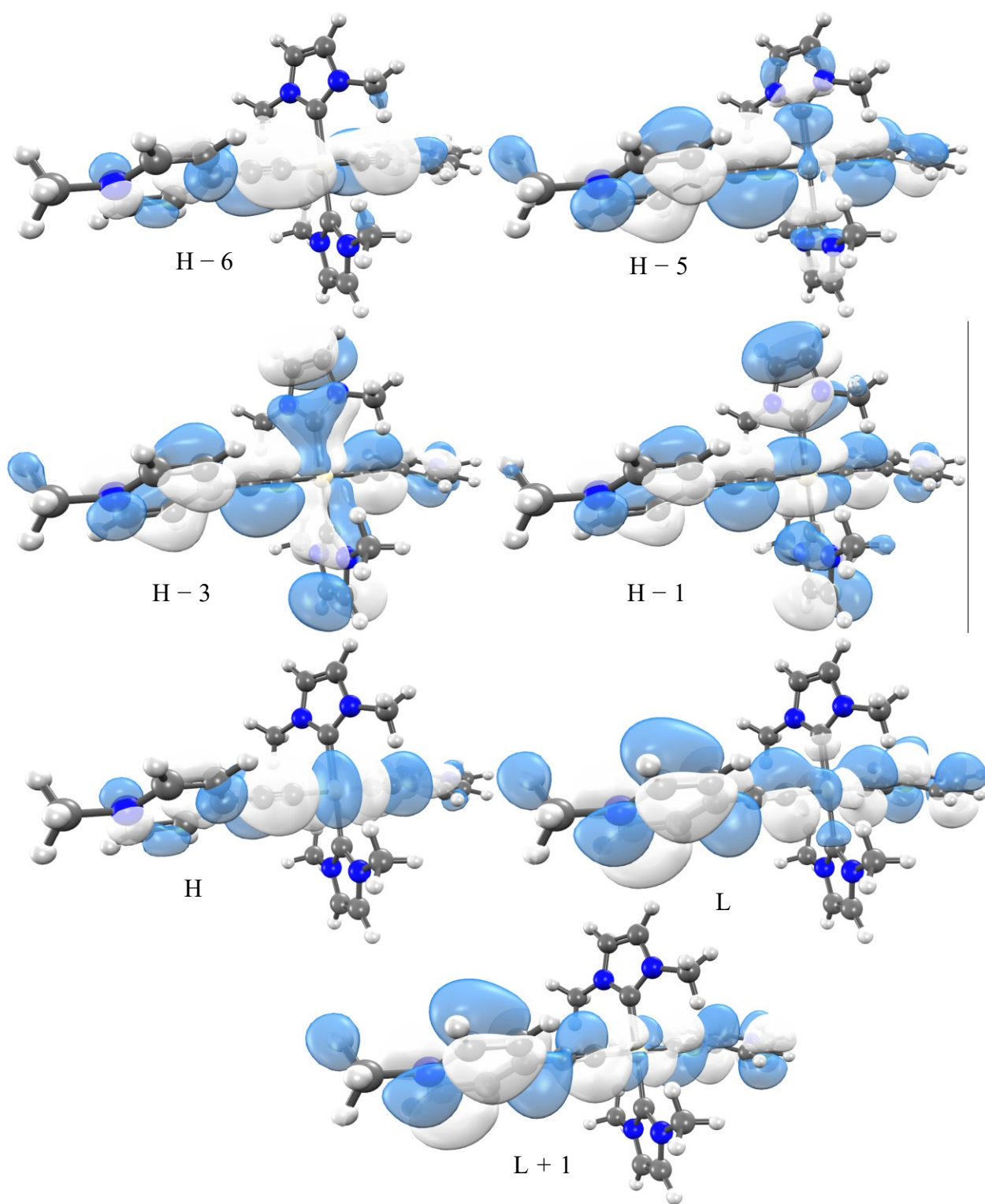


Figure S29. Relevant frontier orbitals for **1-Me**, plotted with an isovalue of 0.04.

Table S8. Natural Population Analysis of **1-Me** in both the ground and excited state.

	Charge in Ground State	Charge in Excited State	Electrons Gained
Platinum	-0.02	0.05	-0.07
Ethynyl Left	-0.24	0.01	-0.25
Pyridyl Left	0.73	0.38	+0.35
Ethynyl Right	-0.24	-0.24	-0.00
Pyridyl Right	0.73	0.63	+0.10
NHC Top	0.51	0.58	-0.06
NHC Bottom	0.51	0.58	-0.06

Table S9. Calculated electronic transition energies of the low-lying singlet excited states of **3**

electronic transition	absorption wavelength/nm (energy/eV)	f	contribution	CI
$S_0 \rightarrow S_1$	309 (4.0082)	0.0004	H - 5 \rightarrow L + 1	0.15505
			H - 1 \rightarrow L	0.66372
			H \rightarrow L + 2	0.12806
$S_0 \rightarrow S_2$	308 (4.021)	0.0069	H - 1 \rightarrow L	0.12386
			H \rightarrow L + 2	0.68938
$S_0 \rightarrow S_3$	299 (4.1529)	0.0000	H - 5 \rightarrow L	0.22367
			H - 1 \rightarrow L + 1	0.63905
			H - 1 \rightarrow L + 4	0.18049
$S_0 \rightarrow S_4$	298 (4.1594)	0.0261	H - 1 \rightarrow L + 2	0.59469
			H \rightarrow L	0.36701
$S_0 \rightarrow S_5$	291 (4.2572)	0.7497	H - 1 \rightarrow L + 2	0.35609
			H \rightarrow L	0.57934
			H \rightarrow L + 3	0.12277
$S_0 \rightarrow S_6$	283 (4.3743)	0.0000	H - 2 \rightarrow L + 3	0.16249
			H \rightarrow L + 1	0.60165
			H \rightarrow L + 4	0.29847
$S_0 \rightarrow S_7$	277 (4.4815)	0.1568	H - 2 \rightarrow L + 1	0.15526
			H - 2 \rightarrow L + 4	0.17125
			H \rightarrow L	0.11706
			H \rightarrow L + 3	0.63028
$S_0 \rightarrow S_8$	276 (4.4875)	0.0000	H - 2 \rightarrow L + 2	0.69993
$S_0 \rightarrow S_9$	274 (4.511)	0.0008	H - 6 \rightarrow L + 3	0.10001
			H - 5 \rightarrow L + 4	0.19264
			H - 1 \rightarrow L + 3	0.65938
			H - 5 \rightarrow L + 3	0.21473
$S_0 \rightarrow S_{10}$	274 (4.5198)	0.0000	H - 1 \rightarrow L + 1	0.18968
			H - 1 \rightarrow L + 4	0.6353

Table S10. Singlet to Triplet Transition Selected to Optimize for **3**

Singlet Transition Modeled	Triplet Transition Selected	Absorption wavelength (nm)	Contribution	CI
5	5	322	H - 6 → L	0.10012
			H - 5 → L + 1	0.22819
			H - 1 → L	0.58266
			H → L + 2	0.25735

Table S11. Ligand and Functional Group Contributions to the Ground State Orbitals of **3**

Orbitals:	H - 6	H - 5	H - 1	H	L	L + 1	L + 2	L + 3
Platinum Contribution	4.4%	0.8%	39.7%	24.3%	1.9%	2.7%	21.3%	0.2%
Carbene Contribution	0.0%	7.0%	5.1%	3.3%	3.6%	1.2%	63.1%	1.9%
Ethynyl Contribution	3.9%	36.8%	43.4%	41.9%	11.8%	7.8%	11.8%	1.9%
Pyridine Contribution	91.7%	55.4%	11.8%	30.5%	82.7%	88.4%	3.8%	96.0%

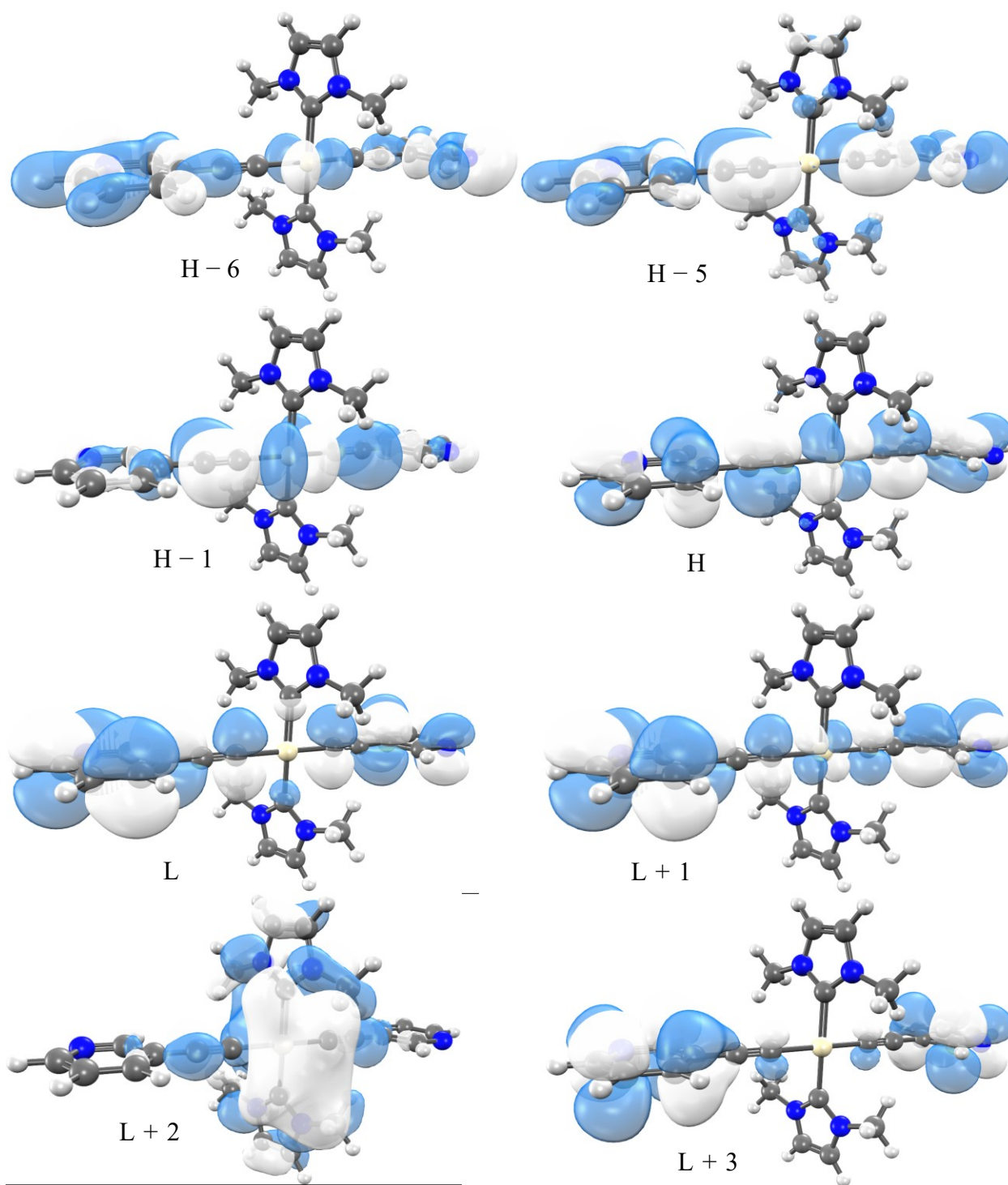


Figure S30. Relevant frontier orbitals for **3**, plotted with an isovalue of 0.04.

Table S12. Natural Population Analysis of **3** in both the ground and excited state.

	Charge in Ground State	Charge in Excited State	Electrons Gained
Platinum	-0.01	-0.11	+0.10
Ethynyl Left	-0.36	-0.25	-0.11
Pyridyl Left	-0.08	-0.14	+0.06
Ethynyl Right	-0.36	-0.25	-0.11
Pyridyl Right	-0.08	-0.14	+0.06
NHC Top	0.45	0.45	0.00
NHC Bottom	0.45	0.45	0.00

Table S13. Calculated electronic transition energies of the low-lying singlet excited states of **3-Me**

electronic transition	absorption wavelength/nm (energy/eV)	f	contribution	CI
$S_0 \rightarrow S_1$	454 (2.7299)	0.0000	H - 1 \rightarrow L	0.69399
$S_0 \rightarrow S_2$	449 (2.7614)	0.0000	H - 6 \rightarrow L	0.10088
			H - 1 \rightarrow L + 1	0.69501
$S_0 \rightarrow S_3$	430 (2.8809)	0.0822	H \rightarrow L	0.70152
$S_0 \rightarrow S_4$	426 (2.9105)	0.0000	H \rightarrow L + 1	0.70008
$S_0 \rightarrow S_5$	380 (3.2629)	0.0000	H - 3 \rightarrow L	0.70411
$S_0 \rightarrow S_6$	379 (3.2676)	0.0453	H - 5 \rightarrow L + 1	0.18193
			H - 2 \rightarrow L	0.66591
			H \rightarrow L + 2	0.12485
$S_0 \rightarrow S_7$	377 (3.2907)	0.0000	H - 5 \rightarrow L	0.19152
			H - 2 \rightarrow L + 1	0.66238
$S_0 \rightarrow S_8$	377 (3.2919)	0.0000	H - 3 \rightarrow L + 1	0.70396
$S_0 \rightarrow S_9$	376 (3.3018)	0.0000	H - 6 \rightarrow L + 3	0.11117
			H - 1 \rightarrow L + 2	0.68653
$S_0 \rightarrow S_{10}$	361 (3.4377)	0.0000	H - 6 \rightarrow L + 2	0.13964
			H - 1 \rightarrow L + 3	0.67743
$S_0 \rightarrow S_{11}$	356 (3.482)	0.0000	H - 4 \rightarrow L	0.70127
$S_0 \rightarrow S_{12}$	353 (3.5087)	0.0000	H - 4 \rightarrow L + 1	0.70594
$S_0 \rightarrow S_{13}$	350 (3.5379)	0.139	H - 5 \rightarrow L + 1	0.45815
			H - 2 \rightarrow L	0.22357
			H \rightarrow L + 2	0.48119
$S_0 \rightarrow S_{14}$	349 (3.5512)	0.0000	H - 5 \rightarrow L	0.65348
			H - 2 \rightarrow L + 1	0.2196
			H \rightarrow L + 3	0.12303
$S_0 \rightarrow S_{15}$	344 (3.5996)	0.2155	H - 5 \rightarrow L + 1	0.48734
			H - 2 \rightarrow L + 2	0.10954
			H \rightarrow L + 2	0.49333

Table S14. Singlet to Triplet Transition Selected to Optimize for **3-Me**

Singlet Transition Modeled	Triplet Transition Selected	Absorption wavelength (nm)	Contribution	CI
13	1	543	H - 5 → L + 1	0.35630
			H - 2 → L	0.33381
			H → L	0.47932

Table S15. Ligand and Functional Group Contributions to the Ground State Orbitals of **3-Me**

Orbitals:	H - 5	H - 2	H	L	L + 1	L + 2
Platinum Contribution	1.3%	9.8%	36.3%	0.1%	0.5%	0.7%
Carbene Contribution	21.8%	45.3%	35.7%	0.6%	0.2%	2.4%
Ethynyl Contribution	49.1%	29.0%	17.1%	1.7%	1.2%	8.9%
Pyridine Contribution	27.7%	15.9%	10.6%	97.7%	98.0%	88.0%

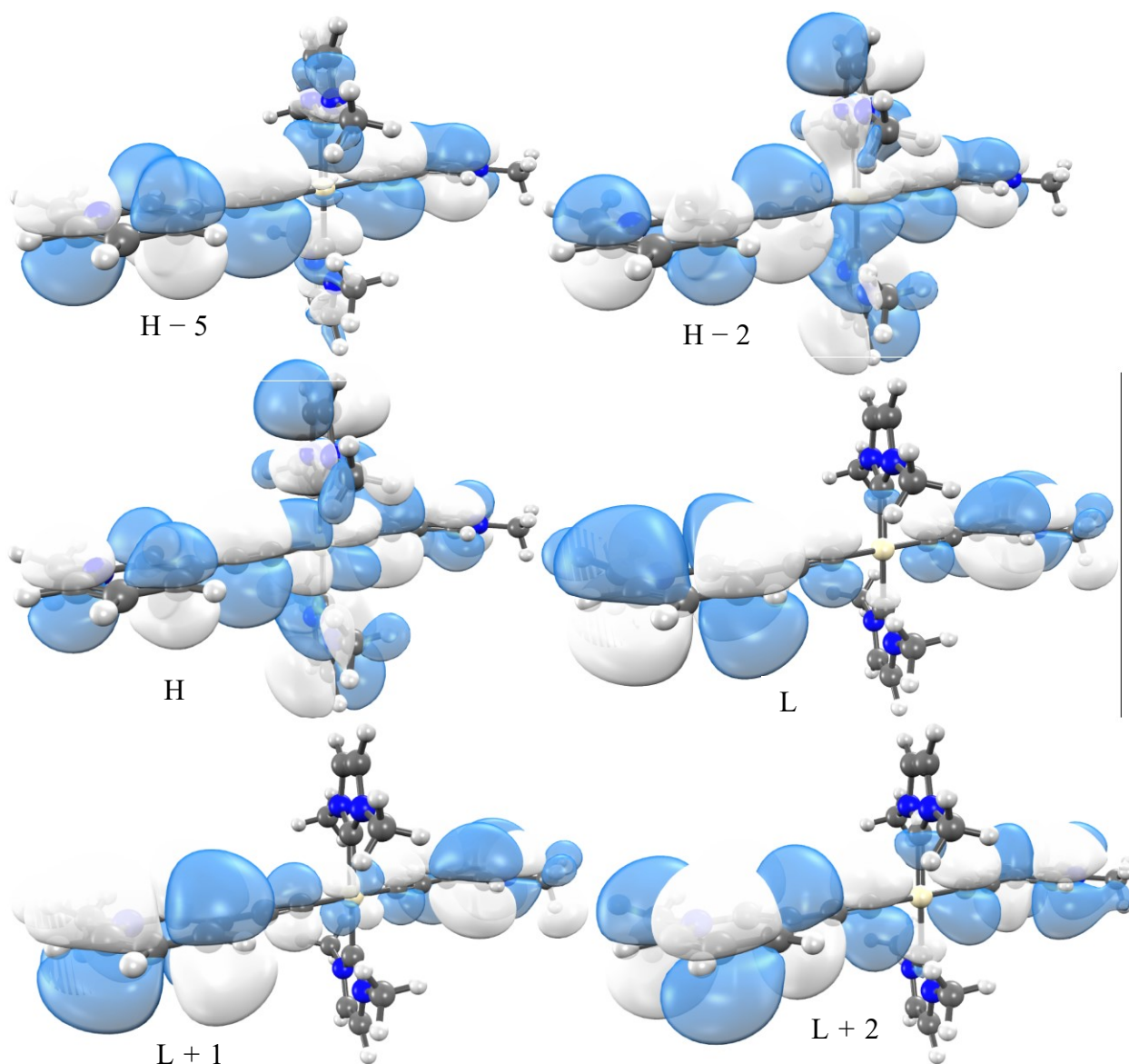


Figure S31. Relevant frontier orbitals for **3-Me**, plotted with an isovalue of 0.04.

Table S16. Natural Population Analysis of **3-Me** in both the ground and excited state.

	Charge in Ground State	Charge in Excited State	Electrons Gained
Platinum	0.00	0.04	-0.04
Ethynyl Left	-0.29	-0.07	-0.22
Pyridyl Left	0.79	0.44	+0.35
Ethynyl Right	-0.29	-0.26	-0.03
Pyridyl Right	0.79	0.82	-0.03
NHC Top	0.50	0.52	-0.02
NHC Bottom	0.50	0.52	-0.02

Table S17. Calculated electronic transition energies of the low-lying singlet excited states of **2**

electronic transition	absorption wavelength/nm (energy/eV)	f	contribution	CI
$S_0 \rightarrow S_1$	313 (3.9637)	0.0000	H - 6 \rightarrow L + 1	0.15586
			H - 1 \rightarrow L	0.68617
$S_0 \rightarrow S_2$	299 (4.1457)	0.0000	H - 6 \rightarrow L	0.20954
			H - 1 \rightarrow L + 1	0.67147
$S_0 \rightarrow S_3$	299 (4.1469)	0.0000	H \rightarrow L + 2	0.70159
$S_0 \rightarrow S_4$	292 (4.2446)	0.0036	H - 1 \rightarrow L + 2	0.58268
			H \rightarrow L	0.38141
$S_0 \rightarrow S_5$	279 (4.448)	1.1942	H - 1 \rightarrow L + 2	0.38324
			H \rightarrow L	0.58525
$S_0 \rightarrow S_6$	278 (4.4674)	0.0000	H - 1 \rightarrow L + 3	0.69858
$S_0 \rightarrow S_7$	272 (4.5598)	0.0000	H - 2 \rightarrow L + 2	0.70137
$S_0 \rightarrow S_8$	268 (4.6226)	0.0000	H \rightarrow L + 3	0.69226
$S_0 \rightarrow S_9$	266 (4.6526)	0.0000	H - 2 \rightarrow L	0.2028
			H \rightarrow L + 1	0.66494
$S_0 \rightarrow S_{10}$	265 (4.6845)	0.0000	H - 5 \rightarrow L + 1	0.32010
			H - 4 \rightarrow L	0.54300
			H - 3 \rightarrow L + 1	0.31210

Table S18. Singlet to Triplet Transition Selected to Optimize for **2**

Singlet Transition Modeled	Triplet Transition Selected	Absorption wavelength (nm)	Contribution	CI
5	4	324	H - 6 \rightarrow L + 1	0.19111
			H - 1 \rightarrow L	0.64472
			H \rightarrow L + 2	0.17550

Table S19. Ligand and Functional Group Contributions to the Ground State Orbitals of **2**

Orbitals:	H - 6	H - 1	H	L	L + 1	L + 2
Platinum Contribution	2.1%	42.6%	22.3%	1.9%	4.3%	24.6%
Phosphine Contribution	2.6%	1.5%	4.5%	8.5%	5.4%	60.3%
Ethynyl Contribution	81.2%	46.1%	44.1%	15.9%	12.3%	10.0%
Pyridine Contribution	14.1%	9.8%	29.0%	73.7%	78.0%	5.1%

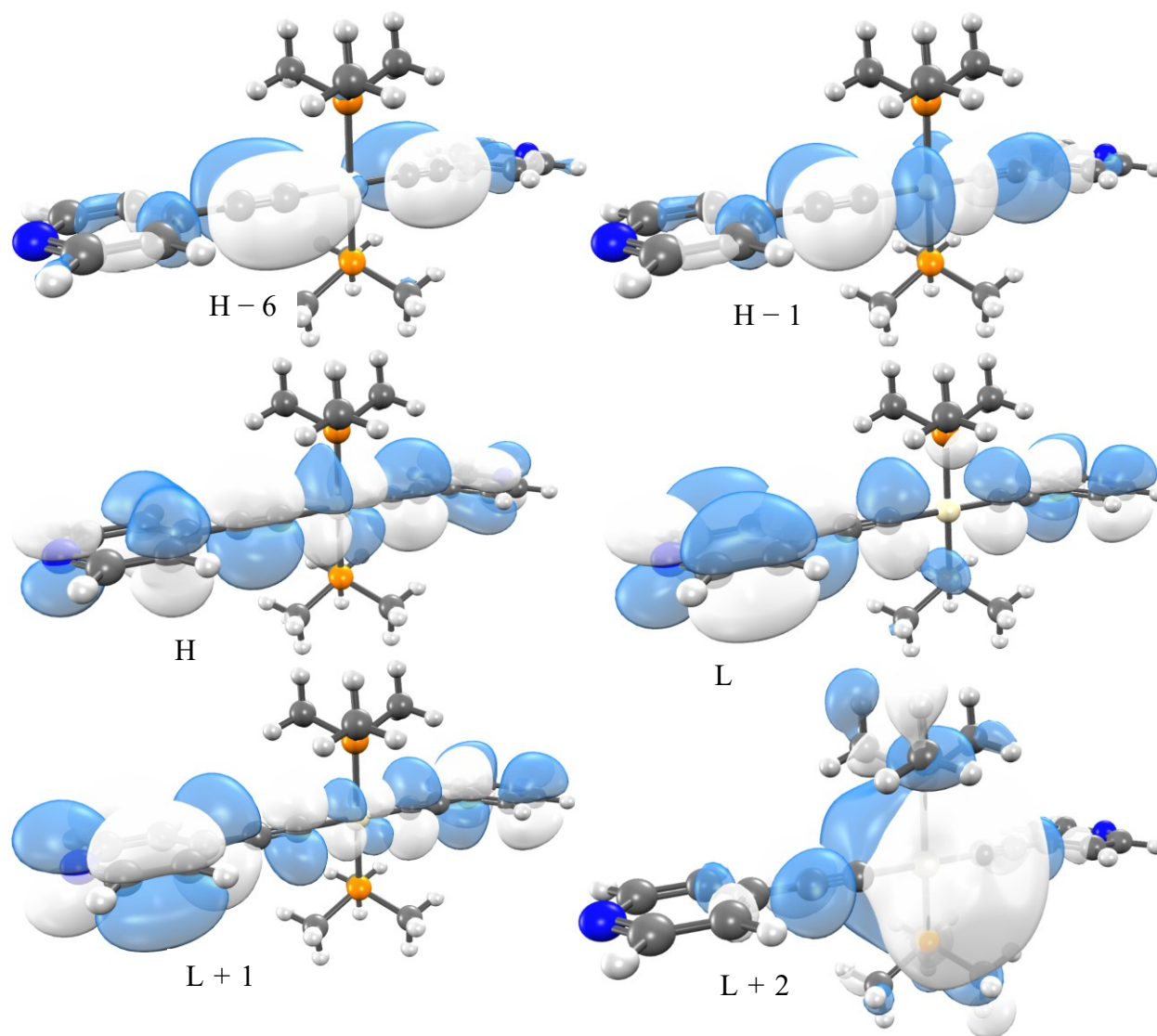


Figure S32. Relevant frontier orbitals for **2**, plotted with an isovalue of 0.04.

Table S20. Natural Population Analysis of **2** in both the ground and excited state.

	Charge in Ground State	Charge in Excited State	Electrons Gained
Platinum	-0.27	-0.33	+0.06
Ethynyl Left	-0.34	-0.20	-0.14
Pyridyl Left	-0.09	-0.21	+0.12
Ethynyl Right	-0.34	-0.32	-0.02
Pyridyl Right	-0.09	-0.09	0.00
NHC Top	0.57	0.58	-0.01
NHC Bottom	0.57	0.58	-0.01

Table S21. Calculated electronic transition energies of the low-lying singlet excited states of **2-Me**

electronic transition	absorption wavelength/nm (energy/eV)	f	contribution	CI
$S_0 \rightarrow S_1$	463 (2.6803)	0.0000	H - 4 \rightarrow L + 1	0.13142
			H \rightarrow L	0.69246
$S_0 \rightarrow S_2$	434 (2.8545)	0.0000	H - 4 \rightarrow L	0.16934
			H \rightarrow L + 1	0.68411
$S_0 \rightarrow S_3$	366 (3.3869)	0.0080	H - 3 \rightarrow L	0.70008
$S_0 \rightarrow S_4$	358 (3.4588)	0.7905	H - 1 \rightarrow L	0.69055
$S_0 \rightarrow S_5$	349 (3.5531)	0.0000	H - 3 \rightarrow L + 1	0.69826
$S_0 \rightarrow S_6$	346 (3.5811)	0.0000	H - 2 \rightarrow L	0.60088
			H - 1 \rightarrow L + 1	0.35649
$S_0 \rightarrow S_7$	329 (3.7723)	0.6381	H - 2 \rightarrow L + 1	0.69269
$S_0 \rightarrow S_8$	322 (3.8540)	0.0000	H - 6 \rightarrow L	0.13804
			H - 2 \rightarrow L	0.34498
			H - 1 \rightarrow L + 1	0.59157
$S_0 \rightarrow S_9$	306 (4.0572)	0.0000	H - 10 \rightarrow L + 1	0.10028
			H - 4 \rightarrow L	0.67604
			H \rightarrow L + 1	0.17300
$S_0 \rightarrow S_{10}$	298 (4.1562)	0.0000	H - 4 \rightarrow L + 3	0.11253
			H \rightarrow L + 2	0.69765

Table S22. Singlet to Triplet Transition Selected to Optimize for **2-Me**

Singlet Transition Modeled	Triplet Transition Selected	Absorption wavelength (nm)	Contribution	CI
4	1	501	H - 6 \rightarrow L + 1	0.16250
			H - 2 \rightarrow L + 1	0.34509
			H - 1 \rightarrow L	0.58704

Table S23. Ligand and Functional Group Contributions to the Ground State Orbitals of **2-Me**

Orbitals:	H - 6	H - 2	H - 1	L	L + 1
Platinum Contribution	11.3%	5.4%	27.9%	0.3%	4.8%
Phosphine Contribution	53.5%	48.1%	2.9%	4.7%	1.9%
Ethynyl Contribution	20.2%	27.9%	40.8%	12.7%	11.3%
Pyridine Contribution	15.0%	18.7%	28.4%	82.4%	82.0%

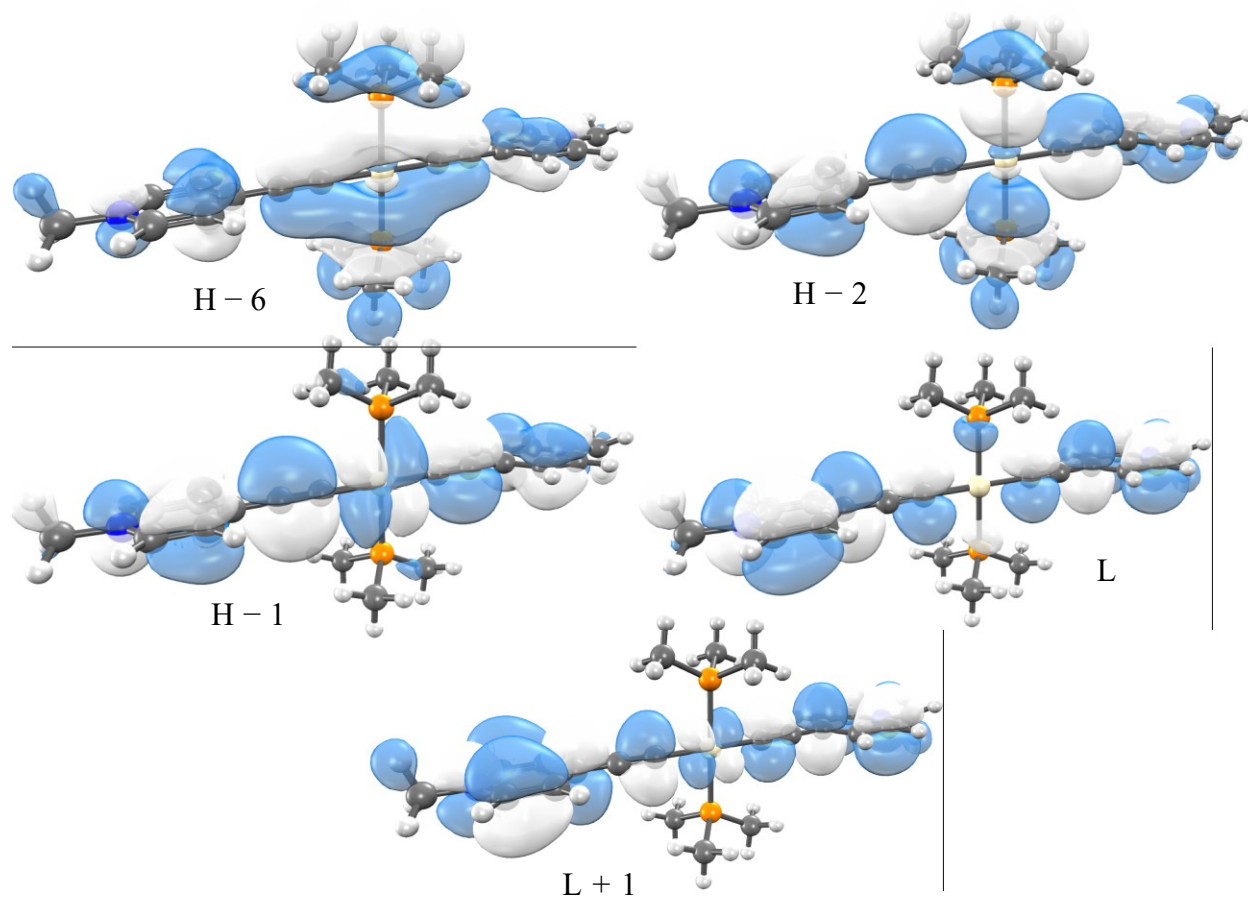


Figure S33. Relevant frontier orbitals for **2-Me**, plotted with an isovalue of 0.04.

Table S24. Natural Population Analysis of **2-Me** in both the ground and excited state.

	Charge in Ground State	Charge in Excited State	Electrons Gained
Platinum	-0.23	-0.19	-0.05
Ethynyl Left	-0.26	-0.09	-0.17
Pyridyl Left	0.76	0.46	+0.30
Ethynyl Right	-0.26	-0.24	-0.02
Pyridyl Right	0.76	0.78	-0.02
Phosphine Top	0.62	0.63	-0.01
Phosphine Bottom	0.62	0.63	-0.01

Table S25. Calculated electronic transition energies of the low-lying singlet excited states of **4**

electronic transition	absorption wavelength/nm (energy/eV)	f	contribution	CI
$S_0 \rightarrow S_1$	311 (3.9892)	0.0001	$H \rightarrow L + 1$	0.69990
$S_0 \rightarrow S_2$	306 (4.0496)	0.0002	$H - 3 \rightarrow L + 2$	0.16685
			$H - 1 \rightarrow L$	0.67285
$S_0 \rightarrow S_3$	295 (4.1973)	0.0000	$H - 3 \rightarrow L$	0.23946
			$H - 1 \rightarrow L + 2$	0.63856
			$H - 1 \rightarrow L + 4$	0.15243
$S_0 \rightarrow S_4$	294 (4.2104)	0.0008	$H - 1 \rightarrow L + 1$	0.59044
			$H \rightarrow L$	0.36591
$S_0 \rightarrow S_5$	284 (4.372)	0.9996	$H - 1 \rightarrow L + 1$	0.34929
			$H \rightarrow L$	0.57361
			$H \rightarrow L + 3$	0.15223
$S_0 \rightarrow S_6$	282 (4.3905)	0.0000	$H - 2 \rightarrow L + 1$	0.70029
$S_0 \rightarrow S_7$	278 (4.4561)	0.0000	$H - 1 \rightarrow L + 5$	0.69177
$S_0 \rightarrow S_8$	277 (4.4787)	0.0000	$H - 2 \rightarrow L + 3$	0.17545
			$H \rightarrow L + 2$	0.59355
			$H \rightarrow L + 4$	0.28748
$S_0 \rightarrow S_9$	276 (4.4957)	0.0000	$H \rightarrow L + 5$	0.69410
$S_0 \rightarrow S_{10}$	270 (4.5851)	0.0029	$H - 5 \rightarrow L + 3$	0.12735
			$H - 3 \rightarrow L + 4$	0.22429
			$H - 1 \rightarrow L + 3$	0.64000

Table S26. Singlet to Triplet Transition Selected to Optimize for **4**

Singlet Transition Modeled	Triplet Transition Selected	Absorption wavelength (nm)	Contribution	CI
5	4	323	$H - 3 \rightarrow L + 2$	0.20814
			$H - 1 \rightarrow L$	0.48200
			$H \rightarrow L + 1$	0.43063

Table S27. Ligand and Functional Group Contributions to the Ground State Orbitals of **4**

Orbitals:	H - 3	H - 1	H	L	L + 1	L + 2	L + 3
Platinum Contribution	0.9%	39.5%	20.5%	1.7%	24.5%	2.8%	0.5%
Phosphine Contribution	1.0%	1.5%	4.5%	7.5%	60.3%	4.0%	2.5%
Ethynyl Contribution	27.3%	43.8%	42.0%	12.9%	9.8%	8.0%	1.9%
Pyridine Contribution	70.8%	15.1%	32.9%	77.9%	5.4%	85.1%	95.2%

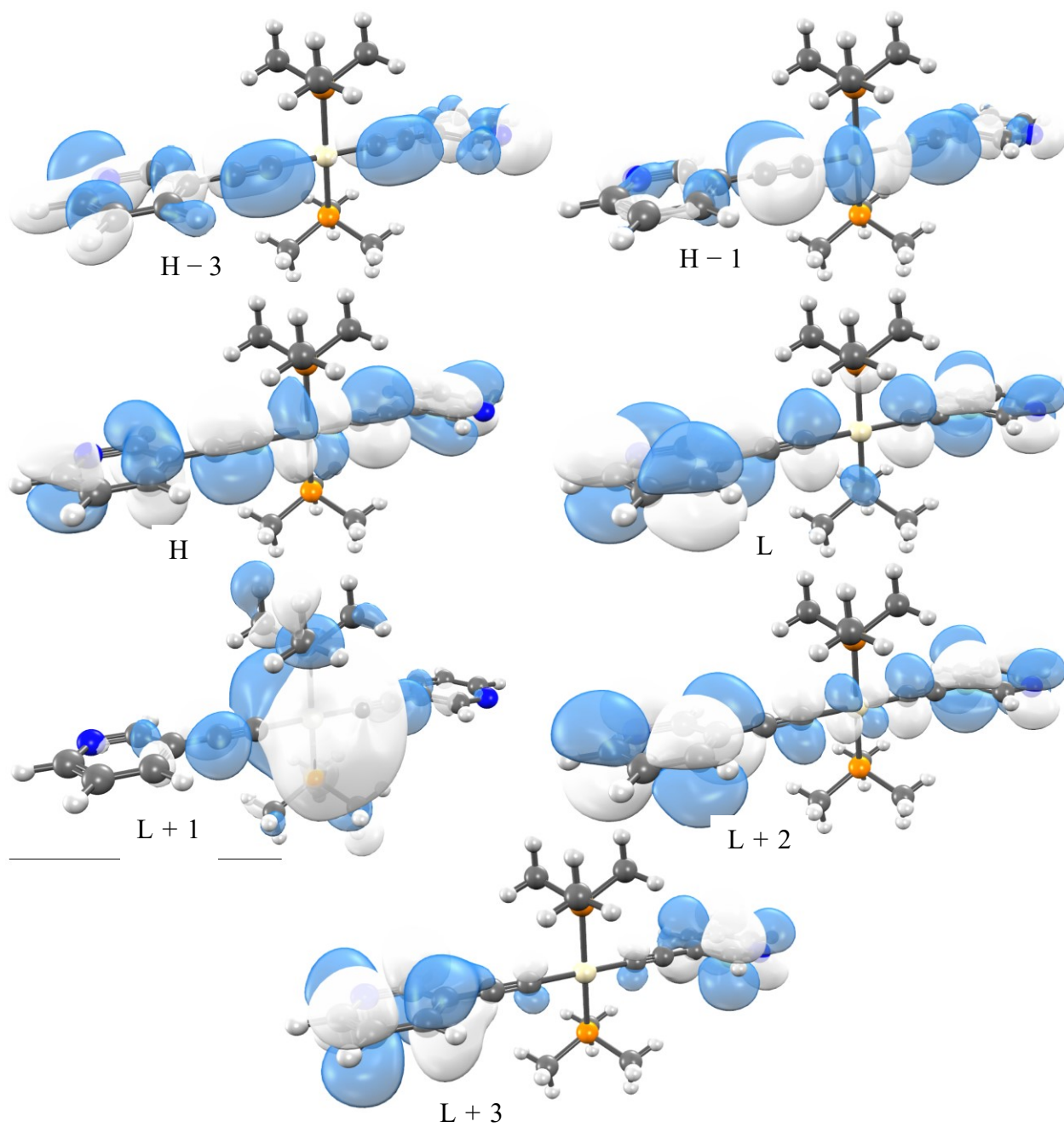


Figure S34. Relevant frontier orbitals for **4**, plotted with an isovalue of 0.04.

Table S28. Natural Population Analysis of **4** in both the ground and excited state.

	Charge in Ground State	Charge in Excited State	Electrons Gained
Platinum	-0.27	-0.33	+0.06
Ethynyl Left	-0.36	-0.23	-0.13
Pyridyl Left	-0.07	-0.18	+0.11
Ethynyl Right	-0.36	-0.34	-0.02
Pyridyl Right	-0.07	-0.07	0.00
Phosphine Top	0.57	0.57	0.00
Phosphine Bottom	0.57	0.57	0.00

Table S29. Calculated electronic transition energies of the low-lying singlet excited states of **4-Me**

electronic transition	absorption wavelength/nm (energy/eV)	f	contribution	CI
$S_0 \rightarrow S_1$	433 (2.8604)	0.0001	$H - 4 \rightarrow L + 1$	0.11249
			$H \rightarrow L$	0.69270
$S_0 \rightarrow S_2$	429 (2.893)	0.0000	$H - 4 \rightarrow L$	0.11926
			$H \rightarrow L + 1$	0.69408
$S_0 \rightarrow S_3$	390 (3.1801)	0.1522	$H - 2 \rightarrow L + 1$	0.18611
			$H - 1 \rightarrow L$	0.67242
$S_0 \rightarrow S_4$	387 (3.2048)	0.0000	$H - 2 \rightarrow L$	0.18951
			$H - 1 \rightarrow L + 1$	0.66677
$S_0 \rightarrow S_5$	364 (3.4056)	0.0001	$H - 4 \rightarrow L + 3$	0.13187
			$H \rightarrow L + 2$	0.68747
$S_0 \rightarrow S_6$	356 (3.4845)	0.0000	$H - 2 \rightarrow L$	0.67183
			$H - 1 \rightarrow L + 1$	0.20502
$S_0 \rightarrow S_7$	355 (3.4948)	0.0055	$H - 2 \rightarrow L + 1$	0.66493
			$H - 1 \rightarrow L$	0.19674
$S_0 \rightarrow S_8$	354 (3.5049)	0.0001	$H - 3 \rightarrow L$	0.69708
$S_0 \rightarrow S_9$	351 (3.5337)	0.0000	$H - 3 \rightarrow L + 1$	0.69691
			$H \rightarrow L + 3$	0.10110
$S_0 \rightarrow S_{10}$	351 (3.5353)	0.0000	$H - 4 \rightarrow L + 2$	0.16340
			$H - 3 \rightarrow L + 1$	0.10512
			$H \rightarrow L + 3$	0.67314

Table S30. Singlet to Triplet Transition Selected to Optimize for **4-Me**

Singlet Transition Modeled	Triplet Transition Selected	Absorption wavelength (nm)	Contribution	CI
3	1	515	$H - 6 \rightarrow L + 1$	0.13490
			$H - 2 \rightarrow L + 1$	0.36608
			$H - 1 \rightarrow L$	0.55815

Table S31. Ligand and Functional Group Contributions to the Ground State Orbitals of **4-Me**

Orbitals:	H - 6	H - 2	H - 1	L	L + 1
Platinum Contribution	11.9%	4.3%	28.2%	0.0%	0.5%
Phosphine Contribution	59.9%	43.5%	3.2%	0.9%	0.5%
Ethynyl Contribution	16.0%	33.4%	43.6%	1.9%	1.2%
Pyridine Contribution	12.3%	18.8%	25.0%	97.2%	97.8%

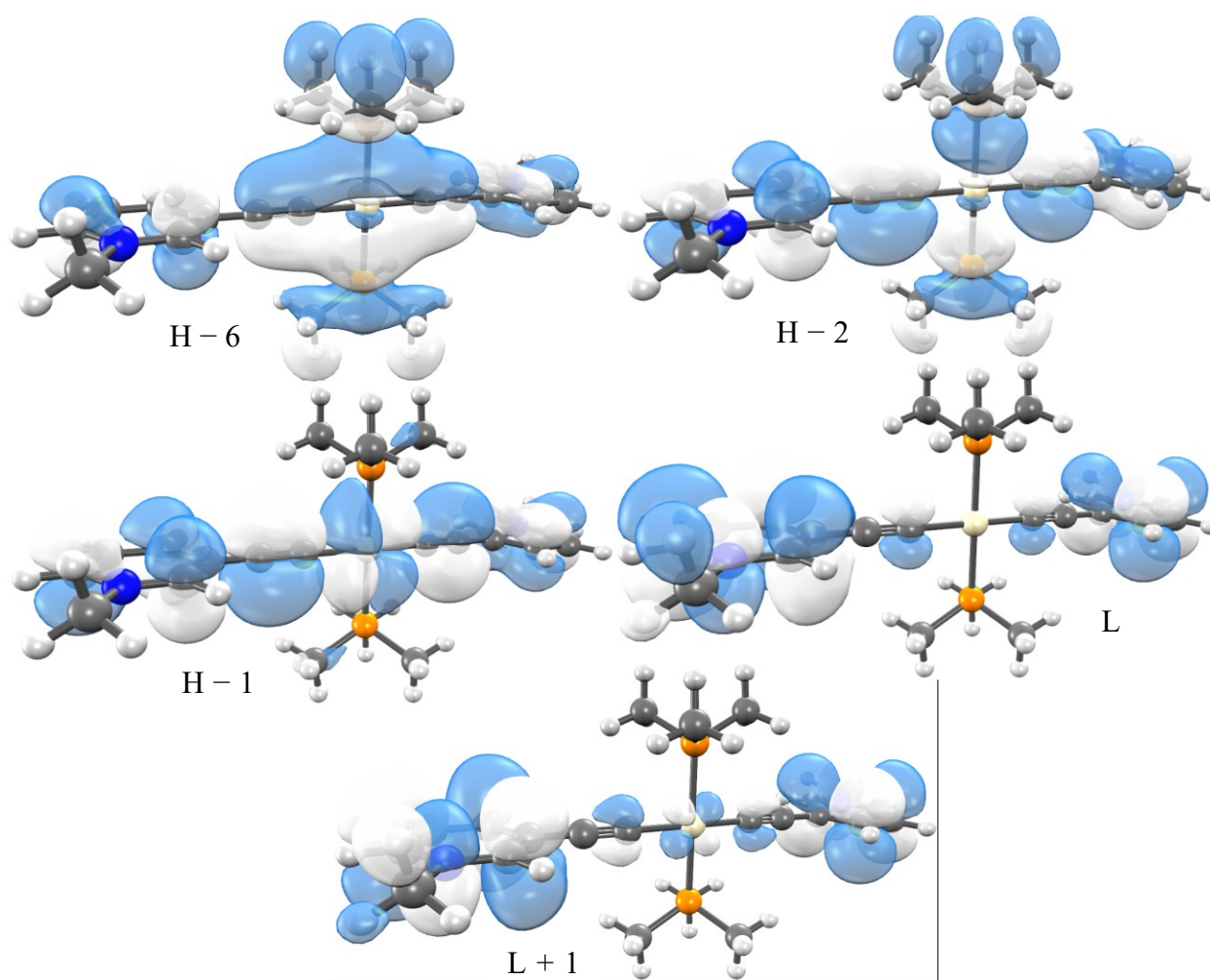


Figure S35. Relevant frontier orbitals for **4-Me**, plotted with an isovalue of 0.04.

Table S32. Natural Population Analysis of **4-Me** in both the ground and excited state.

	Charge in Ground State	Charge in Excited State	Electrons Gained
Platinum	-0.24	-0.19	-0.05
Ethynyl Left	-0.30	-0.10	-0.20
Pyridyl Left	0.81	0.47	+0.34
Ethynyl Right	-0.30	-0.28	-0.02
Pyridyl Right	0.81	0.84	-0.03
Phosphine Top	0.61	0.63	-0.02
Phosphine Bottom	0.61	0.64	-0.03

Crystallographic Details

Single crystals of **2**, **2-Me**, **4**, and **4-Me** were grown as follows: **2** (0.30 x 0.31 x 0.46 mm³, clear, light yellow block) from slow evaporation of methanol, **2-Me** (0.16 x 0.17 x 0.43 mm³ clear, colorless block) from vapor diffusion of diethyl ether into a saturated CH₂Cl₂ solution, **4** (0.12 x 0.12 x 0.28 mm³, clear colorless block) from slow evaporation of a CH₂Cl₂/hexanes solution, and **4-Me** (0.24 x 0.30 x 0.49 mm³, clear yellow block) from vapor diffusion of diethyl ether into a saturated methanol solution. All crystals were suspended in Paratone oil and affixed to a MiTeGen MicroLoop, crystals were mounted on a Bruker D8 Venture diffractometer equipped with an APEX-II CCD detector and molybdenum X-ray source ($\lambda = 0.71073 \text{ \AA}$). Crystals were maintained at 100 K (**2** and **2-Me**) or 106 K (**4** and **4-Me**) for the entirety of data collection. Exposure times of two seconds per frame provided adequate diffraction.

Using Olex2,⁵ initial solutions were obtained for all structures using SHELXS⁶ via direct methods (with the exception of **2-Me** in which structure expansion was employed). Structures were then refined using SHELXL⁷ through least squares minimization. All non-hydrogen atoms were refined anisotropically (with the exception of C5, C6, and N1 in **4**, in this case an ISOR restraint was utilized which allows for isotropic behavior in anisotropically refine atom), hydrogen atoms were located in calculated positions using the standard riding model and refine isotropically. For **4**, C5, C6, and N1 were restrained using SIMU (anisotropic parameter) and DELU (rigid bond) restraints. All other structures refined well and did not warrant the use of any additional restraints. Each complex features a slightly distorted square planar coordination geometry about each Pt center. See Table S33 for further crystallographic information. Both methylated complexes were shown to be charge neutral given the experimentally obtained stoichiometry displayed two triflate counter-ions per complex.

Table S33. Crystallographic Data for **2**, **2-Me**, **4**, and **4-Me**

	2	2-Me · 2OTf	4	4-Me · 2OTf
Empirical formula	C ₂₆ H ₃₈ N ₂ P ₂ Pt	C ₃₀ H ₄₄ F ₆ N ₂ O ₆ P ₂ PtS ₂	C ₂₆ H ₃₈ N ₂ P ₂ Pt	C ₃₀ H ₄₄ F ₆ N ₂ O ₆ P ₂ PtS ₂
Formula weight	635.61	963.82	635.61	963.82
Temperature (K)	99.67	100.0	106.05	105.49
Crystal system	monoclinic	triclinic	monoclinic	monoclinic
Space group	P2 ₁ /n	P-1	P2 ₁ /n	P2 ₁ /n
<i>a</i> (Å)	9.0413(4)	8.9273(5)	8.8056(4)	8.9921(4)
<i>b</i> (Å)	10.8299(5)	8.9819(5)	11.2252(5)	20.8912(9)
<i>c</i> (Å)	14.3021(6)	13.1473(7)	14.0390(7)	10.4273(4)
α (°)	90	75.641(2)	90	90
β (°)	107.367(1)	76.921(2)	106.482(2)	106.284(1)
γ (°)	90	68.656(2)	90	90
Volume (Å ³)	1336.6(1)	940.35(9)	1330.7(1)	1880.2(1)
Z	2	1	2	2
ρ_{calc} (g cm ⁻³)	1.579	1.702	1.586	1.702
μ (mm ⁻¹)	5.384	3.998	5.408	3.999
F(000)	632.0	480.0	632.0	960.0
Crystal size (mm ³)	0.46 × 0.31 × 0.3	0.43 × 0.17 × 0.16	0.28 × 0.12 × 0.12	0.49 × 0.3 × 0.24
Radiation	MoK α (λ = 0.71073)	MoK α (λ = 0.71073)	MoK α (λ = 0.71073)	MoK α (λ = 0.71073)
2 θ range for data collection (°)	7.056 to 56.694	5.732 to 56.776	6.038 to 62.072	5.638 to 62.202
Index ranges	-11 ≤ <i>h</i> ≤ 12, -12 ≤ <i>k</i> ≤ 14, -17 ≤ <i>l</i> ≤ 19	-10 ≤ <i>h</i> ≤ 11, -11 ≤ <i>k</i> ≤ 12, -17 ≤ <i>l</i> ≤ 17	-10 ≤ <i>h</i> ≤ 12, -13 ≤ <i>k</i> ≤ 16, -20 ≤ <i>l</i> ≤ 14	-13 ≤ <i>h</i> ≤ 11, -30 ≤ <i>k</i> ≤ 29, -13 ≤ <i>l</i> ≤ 15
Reflections collected	14476	21959	10281	37739
Independent reflections	3318 [R _{int} = 0.0318, R _{sigma} = 0.0240]	4699 [R _{int} = 0.0421, R _{sigma} = 0.0308]	4155 [R _{int} = 0.0266, R _{sigma} = 0.0404]	6007 [R _{int} = 0.0244, R _{sigma} = 0.0168]
Data/restraints/parameters	3318/0/145	4699/0/227	4155/33/145	6007/0/311
Goodness-of-fit on <i>F</i> ²	1.096	1.095	1.146	1.174
Final R indexes [<i>I</i> ≥ 2 σ (<i>I</i>)]	R ₁ = 0.0167, wR ₂ = 0.0415	R ₁ = 0.0168, wR ₂ = 0.0435	R ₁ = 0.0249, wR ₂ = 0.0532	R ₁ = 0.0177, wR ₂ = 0.0381
Final R indexes [all data]	R ₁ = 0.0207, wR ₂ = 0.0434	R ₁ = 0.0168, wR ₂ = 0.0435	R ₁ = 0.0476, wR ₂ = 0.0752	R ₁ = 0.0233, wR ₂ = 0.0398
Largest diff. peak/hole (e Å ⁻³)	0.51/-1.97	0.85/-1.41	0.82/-1.23	0.41/-1.12

The unweighted R-factor is $R_1 = \sum(F_o - F_c)/\sum F_o$; $I > 2 \sigma(I)$ and the weighted R-factor is $wR_2 = \{\sum w(F_o^2 - F_c^2)^2/\sum w(F_o^2)^2\}^{1/2}$

References:

1. Y. Zhang, C. R. P. Fulong, C. E. Hauke, M. R. Crawley, A. E. Friedman and T. R. Cook, *Chem. Eur. J.*, 2017, **23**, 4532-4536.
2. K. A. Jensen, *Z. Anorg. Allg. Chem.*, 1936, **229**, 252-264.
3. Y. K. Kryschenko, S. R. Seidel, A. M. Arif and P. J. Stang, *J. Am. Chem. Soc.*, 2003, **125**, 5193-5198.
4. M. J. Frisch, G. W. Trucks, H. B. Schlegel, G. E. Scuseria, M. A. Robb, J. R. Cheeseman, G. Scalmani, V. Barone, B. Mennucci, G. A. Petersson, H. Nakatsuji, M. Caricato, X. Li, H. P. Hratchian, A. F. Izmaylov, J. Bloino, G. Zheng, J. L. Sonnenberg, M. Hada, M. Ehara, K. Toyota, R. Fukuda, J. Hasegawa, M. Ishida, T. Nakajima, Y. Honda, O. Kitao, H. Nakai, T. Vreven, J. A. Montgomery Jr., J. E. Peralta, F. Ogliaro, M. J. Bearpark, J. Heyd, E. N. Brothers, K. N. Kudin, V. N. Staroverov, R. Kobayashi, J. Normand, K. Raghavachari, A. P. Rendell, J. C. Burant, S. S. Iyengar, J. Tomasi, M. Cossi, N. Rega, N. J. Millam, M. Klene, J. E. Knox, J. B. Cross, V. Bakken, C. Adamo, J. Jaramillo, R. Gomperts, R. E. Stratmann, O. Yazyev, A. J. Austin, R. Cammi, C. Pomelli, J. W. Ochterski, R. L. Martin, K. Morokuma, V. G. Zakrzewski, G. A. Voth, P. Salvador, J. J. Dannenberg, S. Dapprich, A. D. Daniels, Ö. Farkas, J. B. Foresman, J. V. Ortiz, J. Cioslowski and D. J. Fox, *Journal*, 2009.
5. O. V. Dolomanov, L. J. Bourhis, R. J. Gildea, J. A. K. Howard and H. Puschmann, *J. Appl. Crystallogr.*, 2009, **42**, 339-341.
6. G. Sheldrick, *Acta Crystallographica Section A*, 2008, **64**, 112-122.
7. G. Sheldrick, *Acta Crystallographica Section C*, 2015, **71**, 3-8.